Preliminary evaluation of matrix metalloproteinase-13 selective radiotracers for imaging atherosclerosis

Rami Al Haddad

A thesis submitted in partial fulfillment of the requirements for the master's degree in biochemistry

Department of biochemistry, microbiology and immunology
Faculty of medicine
University of Ottawa

Contents

Acknowledgments

It was a great privilege for me to work with at Dr. Benjamin Rotstein. His constant support, appreciation and persistent motivation are very appreciated. Dr Rotstein's leadership, enthusiasm and knowledge in science were very inspiring to me.

I would like to thank all my lab members: Uzair Sayani, Maxime Munch, Braeden Mair, Gedalliah Farber, and a special thanks to Ariel Buchler, whose chemical synthesis and overall help were key in advancing my project. I am also grateful for my thesis advisory committee members, Dr. Katey Rayner and Dr. Darryl Davis for the invaluable suggestions and comments.

Finally, I would like to express my deepest appreciation to my family. My Fiancée's kindest support, faith, patience and love that have been my greatest source of motivation.

Abbreviations

APMA: 4-Aminophenylmercuric acetate

ApoE: Apolipoprotein E

CAD: coronary artery disease

CD-68: Cluster of differentiation-68

CPM: counts per minute

CT: computed tomography

CVD: cardiovascular diseases

Cys: Cysteine

DLU: digital light unit

ECM: extracellular matrix

FDA: food and drug administration

FDG: fluoro-2-deoxy-D-glucose

Hpx: hemopexin

IC_{50}: 50% inhibitory concentration

ID: injected dose

Lys: Lysine

MMP: matrix metalloproteinase

MRI: magnetic resonance imaging

NaF: Sodium fluoride

NC: normal chow

PET: positron emission tomography

DLU: relative light units

SMC: smooth muscle cells

SPECT: single-photon emission computed tomography

WD: western diet

ZBG: zinc binding group

Zn: Zinc

List of figures and illustrations

List of tables

Abstract

Introduction: Rupture of atherosclerotic plaques is associated with strokes, myocardial infarctions and cardiovascular complications. Collagen, known to be the most abundant protein in atherosclerotic plaques, stabilizes the cap and prevents the lesion from rupture. One of the enzymes responsible for cleaving collagen in plaques is MMP-13. Therefore, we hypothesized that imaging MMP-13 in atherosclerotic plaques using PET radiotracers can be a good indicator in monitoring plaque development and stability.

Results: Our results indicate that developing potent selective MMP-13 inhibitors is possible and radiolabeling these compounds, although challenging, can be a useful tool for imaging MMP-13 in atherosclerotic plaques. Autoradiography and staining techniques show colocalization of our tracer with lipids, an essential indicator of the presence of atherosclerotic lesions. In addition, it was shown that the tracer had similar uptake in both groups of mice, confirmed by PET and biodistribution data. However, more selective MMP-13 tracers need to go though this process. Furthermore, more exclusive atherosclerotic markers should be stained for to confirm that the tracer is most selective for MMP-13.

Conclusion: In conclusion, this study was useful in identifying MMP-13 inhibitors with radiolabeling potential to image MMP-13 in atherosclerotic plaques.

Chapter 1. Introduction

Despite meaningful advances in methods for treating and preventing cardiovascular diseases (CVD), they remain the leading cause of mortality and morbidity around the world, with stroke and ischemic heart disease causing more than 15 million deaths per year around the globe (Figure 1).[1–3] CVD include a wide range of heart and vessel-related conditions of different etiology.[4] These consist of coronary artery disease (CAD), arrythmia, heart failure, heart valve disease, congenital heart disease and cardiomyopathy, among others.[4] CAD is the most common, and is often characterized by the narrowing of blood vessels leading to blood flow abnormalities. CAD is caused by atherosclerosis, and usually affects the vessels supplying blood to the heart.[5] Increasing understanding of the complex roles of calcification, inflammation, and tissue remodeling in CAD and valvular CVD are essential to better understand and classify these conditions.

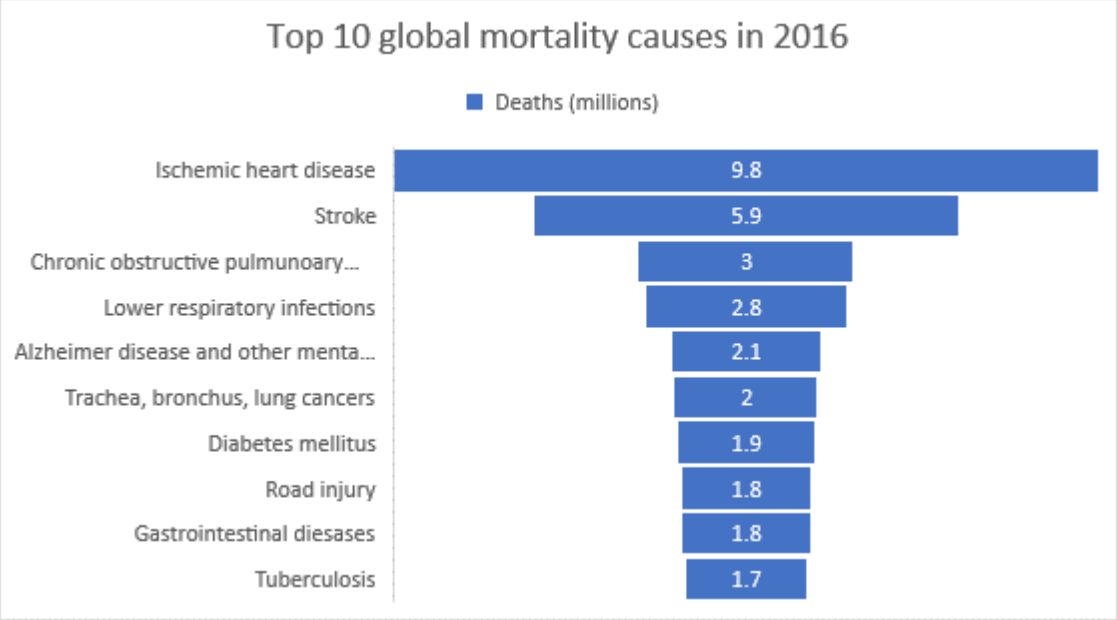

Figure 1: Top 10 causes of mortality worldwide in 2016. Ischemic heart disease and stroke are the 2 leading causes of deaths around the world.[6]

1.1 A brief history of cardiovascular nuclear imaging

Since the early 1900s, an expanding interest in developing new mechanisms and therapeutic strategies directed towards CVD has been emerging, including advances in sensitive and specific diagnostic methods.[7] The birth of the first diagnostic nuclear medicine approach took place in 1927, when Hermann Blumgart and Soma Weiss were successful in their attempt to measure blood circulation time from one arm to another in healthy patients using bismuth-214 (^{214}Bi, $t_{1/2}$ = 26.8 minutes).[8] Almost two decades later, Prinzmetal and colleagues measured the blood transit time between the right and left ventricles, using a Geiger-Müller tube and generating a radiocardiogram after a bolus injection of sodium-24.[9] Following these two studies, a diversity of isotopes and tracers targeting different diseases including oncological applications, musculoskeletal diseases, neurological complications, and cardiovascular diseases have been tested preclinically and clinically to eventually develop currently available and future imaging radiopharmaceuticals.

1.2 PET and other imaging techniques useful for CVD

Nowadays, clinicians have access to various cardiac imaging modalities to diagnose and assess CVD progression in patients.[10] These include echocardiography, X-ray and computed tomography (CT), magnetic resonance imaging (MRI), single-photon emission computed tomography (SPECT), and positron emission tomography (PET).[1,10] PET is a non-invasive imaging technique that measures physiological function by dynamically tracking radiolabelled drugs.[11] One of the biggest advantages of PET is its ability to provide quantitative analyses and to monitor changes in radiolabelled drug distribution over the image acquisition time.[11] The physics behind PET imaging are based on positron emission (β^+) by a neutron deficient isotope.[12] The most commonly used PET isotope is fluorine-18 (^{18}F).[1] As this isotope

decays, the positron is emitted, and travels a short distance at high speeds, eventually interacting with an electron, and both particles get completely annihilated.[12] This produces two high-energy photons that travel in opposite directions and can be detected by the PET scanner.[12] PET detectors are equipped with coincident γ-photon detectors to record decays with high sensitivity. Dynamic and quantifiable images can then be reconstructed with moderate spatial and temporal resolution.[13] Initially, tracers have been developed to detect specific targets at the molecular imaging designed for cancer imaging and atherosclerosis. Images of the radiotracers are reconstructed in 3D, taking scatter, attenuation, deadtime, and random coincidences into consideration.[14] PET imaging is highly sensitive, detecting picomolar concentrations of the tracer.[15] Well-characterized and selective radiopharmaceuticals are the majors contributors in the advances in PET imaging, as they enable exceptional biochemical resolution to probe targets and mechanisms of CVD under different imaging conditions.[5] These tracers, along with ongoing advances in PET technology point toward better tools for diagnosis and assessment of CVD.

1.3 PET radioisotopes

Several factors are taken into consideration when selecting a PET isotope of a clinical CVD pharmaceutical. Its half life must be adequate to the kinetics of tracer distribution and the targeted biochemical processes. Therefore constraints are imposed on the imaging conditions, whether the images are acquired during exercise or in a resting state.[1] In addition, the presence of an on-site cyclotron is required for short-lived radioisotopes such as oxygen-15. Moreover, an ideal PET isotope would decay entirely through positron (β^+) emission.[16] While there is a big selection of PET isotopes with a different physical properties and production methods, the

selection of a nuclide is dependent on molecular structures and synthetic feasibility (Table 1).[17,18]

Isotope	Physical half-life ($t_{1/2}$)	Production	Radiosynthesis
Carbon-11 (^{11}C)	20.34 min	Cyclotron-produced in nitrogen gas: $^{14}N(p,\alpha)^{11}C$	$[^{11}C]CO_2$ or $[^{11}C]CH_4$ precursors, complex synthesis possible
Nitrogen-13 (^{13}N)	9.96 min	Cyclotron-produced in water: $^{16}O(p,\alpha)^{13}N$	$[^{13}N]NH_3$ or $[^{13}N]NO_3^-$ precursors, complex synthesis uncommon
Oxygen-15 (^{15}O)	2.04 min	Cyclotron-produced in nitrogen gas: $^{14}N(d,n)^{15}O$ or $^{15}N(p,n)^{15}O$	$[^{15}O]O_2$ is most common precursor, single-step synthesis possible
Fluorine-18 (^{18}F)	109.7 min	Cyclotron-produced in enriched water: $^{18}O(p,n)^{18}F$	$[^{18}F]$fluoride most common precursor, complex synthesis possible
Copper-64 (^{64}Cu)	12.7 h	Cyclotron-produced: $^{64}Ni(p,n)^{64}Cu$	Chelation chemistry

Gallium-86 (^{68}Ga)	67.8 min	Generator-produced from germanium-68	Chelation chemistry
Rubidium-82 (^{82}Ru)	1.25 min	Generator-produced from strontium-82	Used as eluted

Table 1: Different isotopes available for radiolabeling targets used in PET imaging.[1]

1.4 Atherosclerosis

1.4.1 Progression of the disease

Atherosclerosis is a slowly progressive disease that leads to heart and vessels related complications.[19] It is a disease of the vascular intima that can induce complications in different arteries, mainly the coronary arteries of the heart.[20] Atherosclerosis is characterized by the accumulation of fibrous elements and lipids in the large arteries.[21] Early on, subendothelial accumulations of macrophages filled with cholesterol, also known as foam cells, cause the characteristic lesions of atherosclerosis.[19] Fatty streaks alone are considered clinically insignificant, however, their presence signals the possibility of advanced lesions distinguished by the accumulation of lipid-rich necrotic debris in addition to smooth muscle cells (SMCs).[19] Intermediate lesions are then formed by extracellular lipid accumulation. However, the formation of the fibrous plaques starts with the increased amount of cholesterol deposited in the intima and its underlying smooth muscle cells layer.[22] These lesions have a fibrous cap that is formed of extracellular matrix (ECM), proteoglycans, SMCs, and collagen fibrils enclosing the lipid-rich necrotic core and maintaining the rigidity of the

atherosclerotic cap.[21] Atherosclerotic plaques are subject to an increase in complexity: they are prone to calcification and luminal surface ulceration. Furthermore, small vessels originating from the media of the blood vessel wall can grow into the fibrous lesions causing severe hemorrhage.[23] Advanced lesions may cause stenosis and even completely block blood flow.[20] A wide variety of events weaken the integrity of the cap resulting in a vulnerable advanced atherosclerotic plaque; these include: increased inflammation, tissue proteolysis, and mechanical stress.[24] The most significant clinical risk for the cascade of vascular modification is the acute occlusion of the artery caused by a blood clot or thrombus, leading to a myocardial infarction or stroke. This is most common after rupture of a lesion (Figure 2).[19,25] Numerous markers of atherosclerosis have been identified and are being exploited by different studies to assess the degree of disease progression.[22]

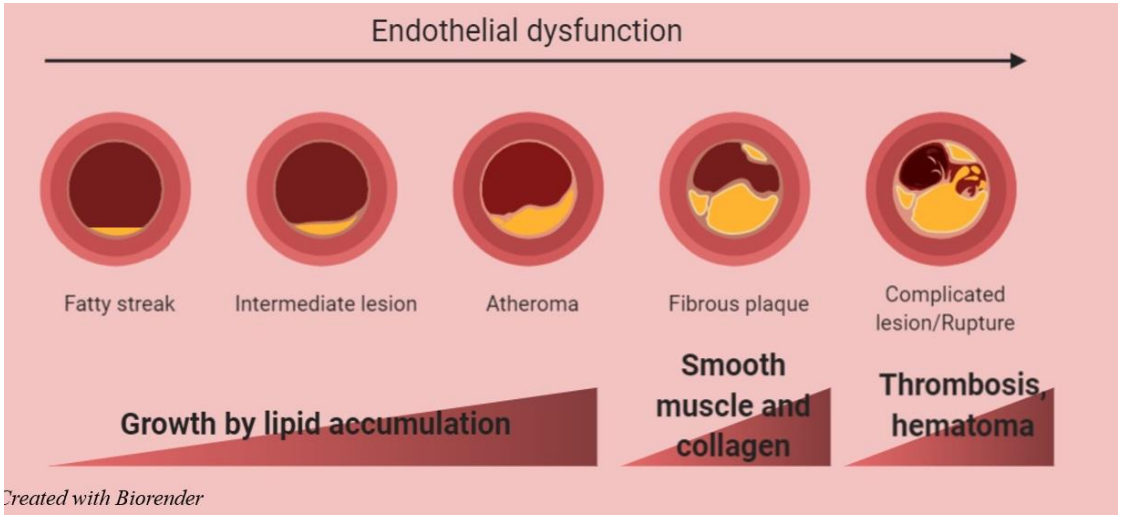

Figure 2: Schematic representation of the stages of atherosclerosis.[26]

1.4.2 Atherosclerotic plaque composition

Atherosclerotic caps are mainly composed of smooth muscle cells, macrophages, cholesterol, and extracellular matrix (ECM) that largely participates in most of the features of the atherogenic process.[27] The main component of the ECM is collagen, the largest contributor in maintaining the atherosclerotic cap integrity and rigidity.[28] Collagen, the most abundant protein in the animal kingdom, is the major insoluble fibrous protein in the ECM.[28] At least 16 types of collagen are known, but 80-90% of collagen in the human body consists of types I, II, and III. The ability of collagen molecules to pack together and form similar structures of long thin fibrils allows collagen to contribute to the rigidity of the different structures.[28,29] The disruptions in collagen content in any tissue are strongly correlated with pathophysiological consequences caused by the loss of structural integrity of the tissue.[27] This is seen in atherosclerosis, where the plaque vulnerability is dependent on its collagen content.[27,30] In addition to the production of collagen in atherosclerotic plaques by SMC, collagen can also be secreted by endothelial cells.[31] During the progression of the disease, SMC shift from their quiescent phenotype to a proliferative matrix synthetic phenotype, abundantly secreting collagen.[32] Among the 3 types of collagen found in plaques, collagen III seems to be the most abundant, with an average of 61% in patient endarterectomy specimens (Table 2).[27]

Collagen type	Principal tissue distribution	Cells of origin
I	Loose and dense connective tissue Bone Fibrocartilage	Fibroblasts and reticular cells Osteoblast
II	Hyaline and elastic cartilage	Chondrocytes

	Vitreous body of the eye	Retinal cells
III	Loose connective tissue, reticular fibers Papillary layer of dermis	Fibroblasts and reticular cells
	Blood vessels	Smooth muscle cells, endothelial cells
IV	Basement membranes	Epithelial and endothelial cells

Table 2: Different types of collagen. Tissue biodistribution and cells of origin.[27]

1.5 Matrix Metalloproteinases and atherosclerosis: The role of MMP-13 in vulnerable plaques

One of the most important features of development and tissue repair is the timely degradation of ECM.[33,34] In healthy conditions, ECM degradation is kept under tight regulation, however, a wide array of diseases is caused when it becomes dysregulated. These include arthritis, nephritis, cancer, and others. Moreover, if ECM remodeling goes uncontrolled in the vasculature and myocardium, it leads to cardiovascular pathology: heart failure, left ventricular hypertrophy, atherosclerosis, and others.[33–35] As mentioned previously, collagen is the main component of the ECM.[36] It allows the maintenance and stability of the organs, supporting their structural integrity.[36] Matrix metalloproteinases (MMP) are a large family of Zn^{2+}- dependent endopeptidases that are known for cleaving collagen. The expression of MMP genes is significantly higher in connective tissue cells, monocytes, endothelial cells, and macrophages.[37] At physiologically healthy conditions, MMPs are expressed at baseline levels, however, in response to certain hormones or cytokines, their expression changes differentially. Most MMPs have a typical conserved structure: an 80-amino acid propeptide, a 170-amino

acid catalytic domain, and a hinge region that links this domain to a 200-amino acid hemopexin domain (Hpx) (Figure 3).[38] Among more than 20 MMPs known to be present in humans, many of them are found in the vascular system.[39] Some have shown to positively affect the plaques, others have a negative impact, and a few of them have alternating effects as the disease progresses to further stages.[40] MMP-1, also known as fibroblast, plays a role in preventing microcalcification, producing smaller and more stable plaques, while MMP-2 (gelatinase A) knockout mice have shown unstable plaques and fewer SMCs than macrophages, highlighting the positive role of these 2 MMPs in atherosclerosis.[41,42] On the other hand, MMP-3, also known as stromelysin-1, is known to act on E-cadherin and stromleysin to restore migration of SMC.[40] However, two different effects where seen upon knockout of MMP-3: in the aorta, larger and more stable plaques were found, however, larger and less stable plaques were found in the brachiocephalic artery.[43,44] These divergent effects are also seen in MMP-7, MMP-9, and MMP-12.[43]

MMP-13 (collagenase-3) inhibition has been shown to increase plaque collagen content in the plaque.[45,46] The main substrate for MMP-13 is type III collagen, the most abundant type of collagen in the atherosclerotic plaque and the largest contributor to its stability.[27,45] In addition, studies has shown and increase of type III collagen in plaques upon inhibition or knockout of MMP-13.[45–47] Therefore, MMP-13 is one of the major collagen degrading enzymes responsible for the vulnerability of the atherosclerotic plaque.

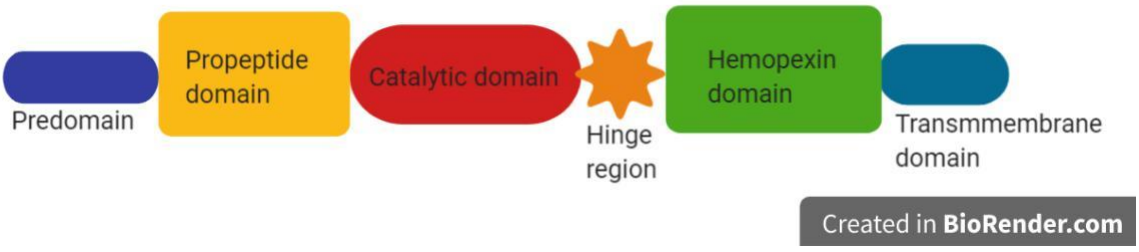

Figure 3: General conserved structure of MMPs.[48]

1.5.1 MMP activation

The most common structural signatures in MMPs are a zinc binding motif in the propeptide domain and a zinc binding motif in the catalytic domain. MMPs are synthesized as pre-proenzymes and the predomain is removed during translation to generate the proMMPs. [38] Similar to other protein synthesized as proenzymes, the propeptide needs to be cleaved to have a fully active enzyme. [49] Three histidine amino acids in the zinc binding motif of the propeptide domain coordinate with the zinc ion in the catalytic site, keeping proMMPs inactive by creating a barrier for a water molecule essential for catalysis of the Cys-Zn^{2+} bond. This is known as the cysteine switch, and it lies in the substrate binding pocket. Once the Cys-Zn^{2+} sulfide bond is disrupted, a water molecule replaces the sulfide group, resulting in an intermediate active form, where autoproteolysis will occur, displacing the propeptide domain.[50] Therefore, it is necessary to activate every MMP using zinc-chelating agents that can disrupt the Cys-Zn^{2+} sulfide bond, rendering MMPs active (Figure 4).

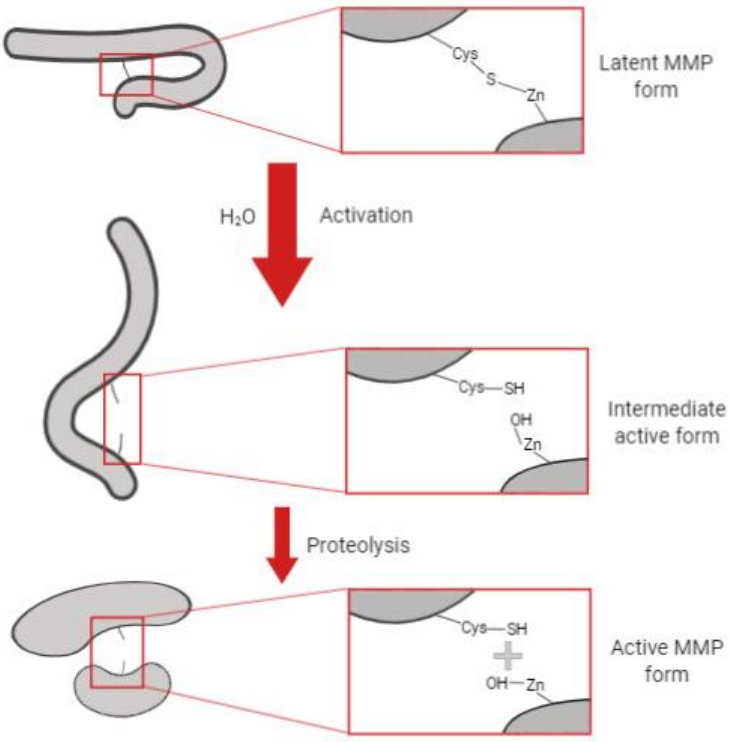

Figure 4: MMP-13 activation mechanism. A water molecule initiates the activation of the latent MMP, resulting in an intermediate active form. The MMP then attains its active form by proteolysis and release of the propeptide domain. Cys: Cysteine, Zn: Zinc.[50]

1.5.2 MMP mechanism of action

MMP substrates bind to the catalytic domain of the enzyme. The carbonyl group of the peptide bond to be cleaved is placed in the catalytic site.[38] The length and structure of the substrate dictate its docking to the catalytic site where it binds to an S1' pocket, located close to the zinc cation. This pocket is known to vary in depth in each MMP, therefore, it is a key factor determining MMP specificity to its targets.[38] Among different MMPs highly expressed in atherosclerotic plaques, MMP-13 cleaves collagen-III, the most abundant type of collagen in the atherosclerotic plaque, therefore, contributing to the instability of the plaque and increasing the incidence of its rupture.[50] MMP-13 has 2 pockets that are characteristic to this enzyme and were not found in any other MMP. The S1' pocket in MMP-13 is particularly large and when a proper ligand binds, it opens a side pocket known as the S1'*, a phenomenon that is not observed in all other MMPs.[51] Since the zinc cation is essential for the activity of all members of the MMP family, MMP inhibitors' interaction with zinc tends to decrease MMP inhibitor selectivity. Therefore, the S1' and S1'* binding pockets are subjects of current extensive research to synthesize novel more potent and selective MMP-13 inhibitors (Figure 5).[52]

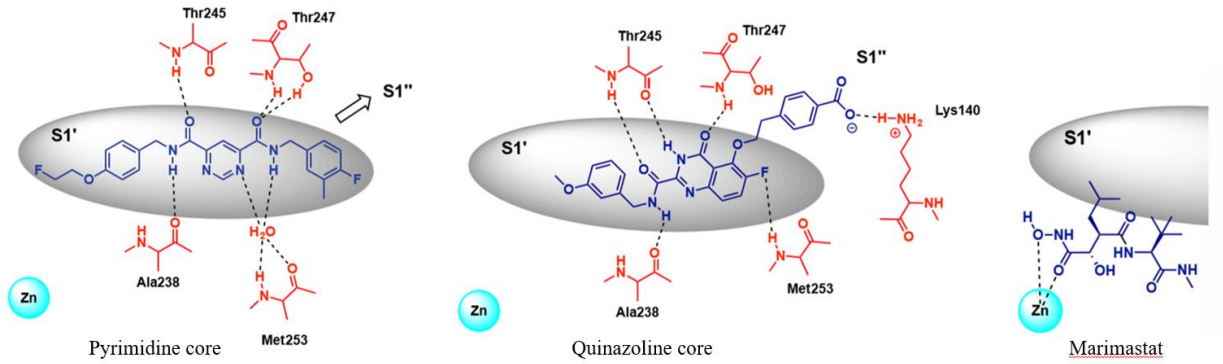

Figure 5: Key interactions of different inhibitors with the S1' binding pocket in MMP-13.[51,53]

1.6 Previous PET tracers targeting MMPs

1.6.1 [^{18}F]FDG: an inflammation marker

[^{18}F]fluoro-2-deoxy-d-glucose or [^{18}F]FDG is the most widely used PET tracer for a variety of diseases.[54] In particular, [^{18}F]FDG uptake has been validated as a marker of atherosclerotic plaque inflammation.[55] [^{18}F]FDG is taken up by different cells and goes through phosphorylation by hexokinase, however unlike glucose, it does not complete the glycolysis pathway.[56] Therefore, the tracer is trapped in the cytoplasm and serves as a marker for high metabolic energy consumption when high tracer density is detected.[55] Moreover, studies show a strong correlation between high [^{18}F]FDG uptake and expression of other inflammation markers, notably macrophages.[57,58] Therefore, [^{18}F]FDG serves as an inflammatory marker and can be useful in assessing atherosclerosis progression because high metabolic activity is present in sites of inflammation. However, the main disadvantage of [^{18}F]FDG uptake is its lack of specificity, as the tracer is known to bind to inflammatory macrophages among other cell types, in addition to showing high uptake in organs with high metabolic activity, such as the heart. Consequently, myocardial uptake masks the signal in vascular plaques.[1] Therefore, other

markers that are more specific to targets in atherosclerotic plaques are needed to identify inflammation in atherosclerotic plaques using PET.[59]

1.6.2 [^{18}F]NaF: a calcification marker

Another marker for detection of the progression of atherosclerosis and lesion vulnerability is calcification of atherosclerotic caps. Unlike microcalcifications, macrocalcifications are markers of stable plaques.[60] Microcalcifications can increase the risk of plaque rupture by amplifying the mechanical stress in the atherosclerotic cap by more than 500 kPa.[61] [^{18}F]NaF has been approved by the FDA as a PET tracer and is being used clinically, as it can bind to microcalcification regions in atherosclerotic plaques.[60] Moreover, it is considered to be a specific marker of active microcalcification since it binds to hydroxyapatite by replacing its hydroxyl groups.[62]

Although [^{18}F]FDG and [^{18}F]NaF are being used clinically, their lack of specificity is a source of concern. Therefore, a need to develop a more specific marker arises. MMP-13, being the most abundant in atherosclerotic plaques, and the largest contributor to the rigidity and integrity of the plaque seems to be a promising target for imaging to assess the risk of development of the disease from the early lesions to the advanced atherosclerotic plaque.

1.7 Aims and objectives

First, using an enzyme assay, the IC_{50} values of the inhibitors synthesized in the lab needed to be determined in order to select the most potent and selective MMP-13 inhibitor for future animal studies. For this assay, 2 groups of inhibitors with different cores were used: the

first is the pyrimidine core, and the second is the quinazoline core (Figure 6). Several functional groups have been added to these cores, creating numerous derivatives.

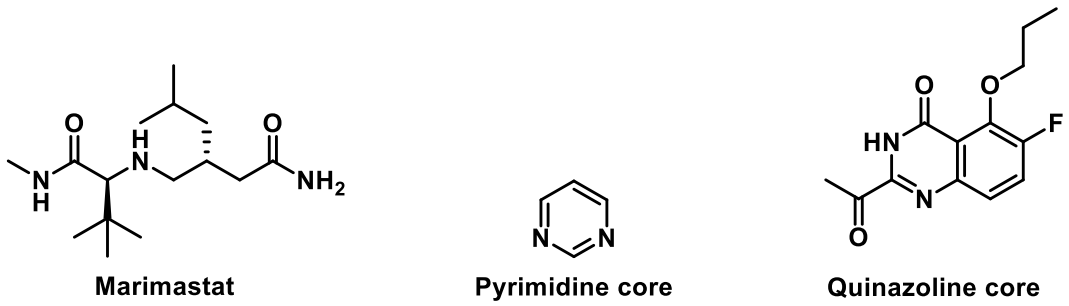

Figure 6: Chemical structures of Marimastat, a Pyrimidine core, and a Quinazoline core

Second, the inhibitors needed to be labeled with fluoride-18 and eluted in saline to make it suitable for mouse injection. The first inhibitor to be radiolabeled was P1, as it was the first to be synthesized and tested, and its precursor (P0), shown in figure 7, was a convenient candidate for fluoride-18 labelling due to its good leaving group. Labelling the inhibitor is of extreme importance for future *in vivo* and *ex vivo* studies. It can serve as an efficient tool in autoradiography techniques and PET imaging. This radiolabeling method was developed in the lab and more inhibitors are now in queue for radiolabeling attempts either with flurorine-18 or carbon-11.

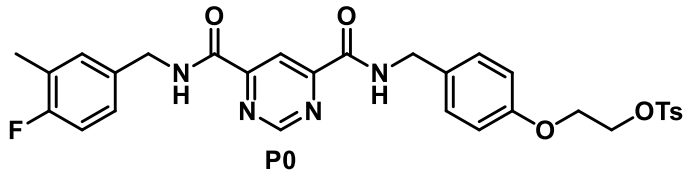

Figure 7: Chemical structure of P0

Third, colocalization studies on harvested en face aortas were necessary to localize the tracer uptake in the aorta and correlate it with markers of atherosclerosis. A mouse model with increased atherosclerotic plaque incidence is compared to a non-diseased mouse. The

radiolabelled P1 is tested here as a marker for atherosclerotic lesions, and a well-established staining technique is applied to validate the observations.

Finally, to determine the tissue distribution of the tracer, PET scans are acquired and biodistribution studies are performed. Here, different techniques enabling us to visualize the tracer in the aortic arch are attempted. Moreover, these are ways to check for difference in tracer metabolism in both animal models used.

The overall aims and objectives for this project were to show that due to the relationship between MMP-13 and atherosclerosis discussed previously, MMP-13 potent and selective inhibitors can provide an efficient tool in tracking the vulnerability of atherosclerotic lesions. In the long term, MMP-13 can be used as an imaging marker to assess the risk of progression of atherosclerosis plaques towards more vulnerable lesions with thinner atherosclerotic cap.

1.8 Rationale and hypothesis

Due to the relationship between atherosclerosis and MMP-13, this enzyme can be crucial in tracking the vulnerability of atherosclerotic lesions and therefore can be used as an imaging marker for risk of progression of atherosclerosis.

Chapter 2: Materials and methods

2.1 *In vitro* enzyme assay:

To test the potency and assess the selectivity of the newly synthesized inhibitors, an enzyme assay was developed using recombinant human MMPs (rhMMP-1, -2, -8, -9, -20, and -13). Recombinant human proteins are generated following isolation of the expressed portion of the DNA (mRNA), reverse transcribing it to cDNA, and then expressing it in other rapidly multiplying organisms such as bacteria.[65] An MMP fluorogenic substrate (MCA-Lys-Pro-Leu-Gly-Leu-DNP-Dpa-Ala-Arg-NH2) is also used for this assay (Figure 8). This substrate is tagged with a donor and a quencher.[66] Upon excitation at λ = 320 nm, the quencher dampens the signal emitted and it does not get detected by the sensors on the Synergy HT fluorescent 96-well plate reader. After the substrate is cleaved, the donor and quencher are separated, and the donor emits a wavelength detected by the fluorescent sensor. Therefore, the higher the fluorescence, the higher the enzyme activity, and the lower efficiency (higher IC_{50} of the inhibitor and/or the concertation used. This is useful in choosing which inhibitors to radiolabel for *in vivo* experiments. It is essential to synthesize a potent and selective MMP-13 inhibitor to eliminate off-target binding in animal models and validate the tracer as specific for MMP-13 only. Twelve inhibitors were synthesized, purified, and tested for potency against different enzymes. These inhibitors were tested and compared to Marimastat as a control, a pan MMP inhibitor, and the first inhibitor to enter MMP clinical testing.[63] It is a hydroxamic acid analog shown in figure 6, and known to be a good zinc-binding group (ZBG).[64] Upon water encounter, the hydroxamate ion potently binds to Zn^{2+} causing its chelation.[64] What makes Marimastat more effective is the ability of hydroxamates to form hydrogen bonds between the ZBG and other amino acid residues.[64]

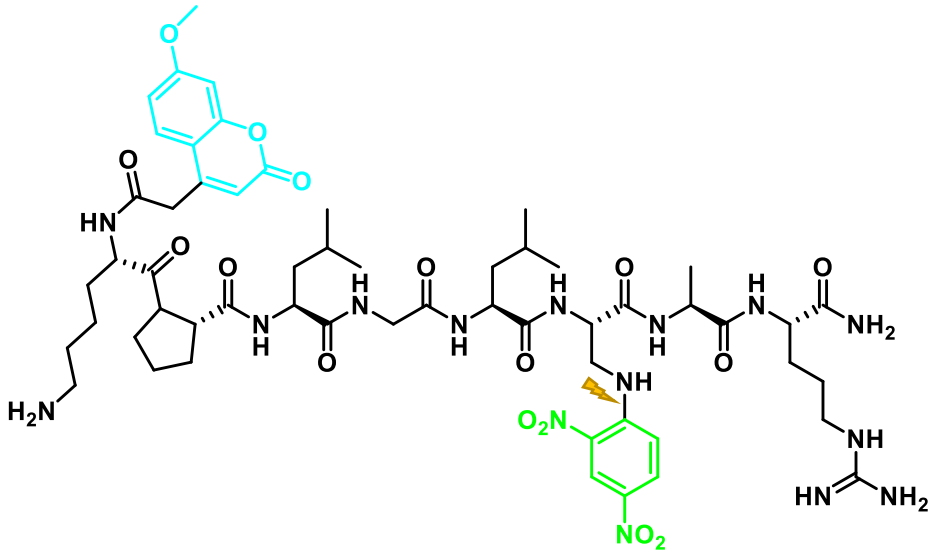

Figure 8: Chemical structures of the fluorogenic MMP substrate used in the enzyme assays. The MCA (fluorophore) is shown in blue, while DNP (quencher) is shown in green. The yellow lighting mark shows the cleavage site by MMPs, releasing the fluorophore from the rest of the molecule.[66–68]

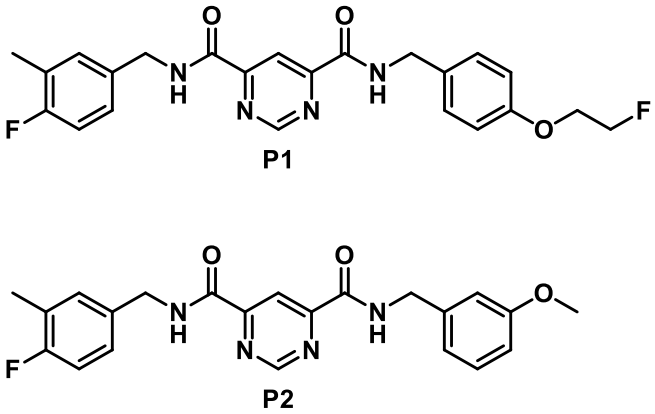

Figure 9: Chemical structures of Pyrimidine core-based inhibitors

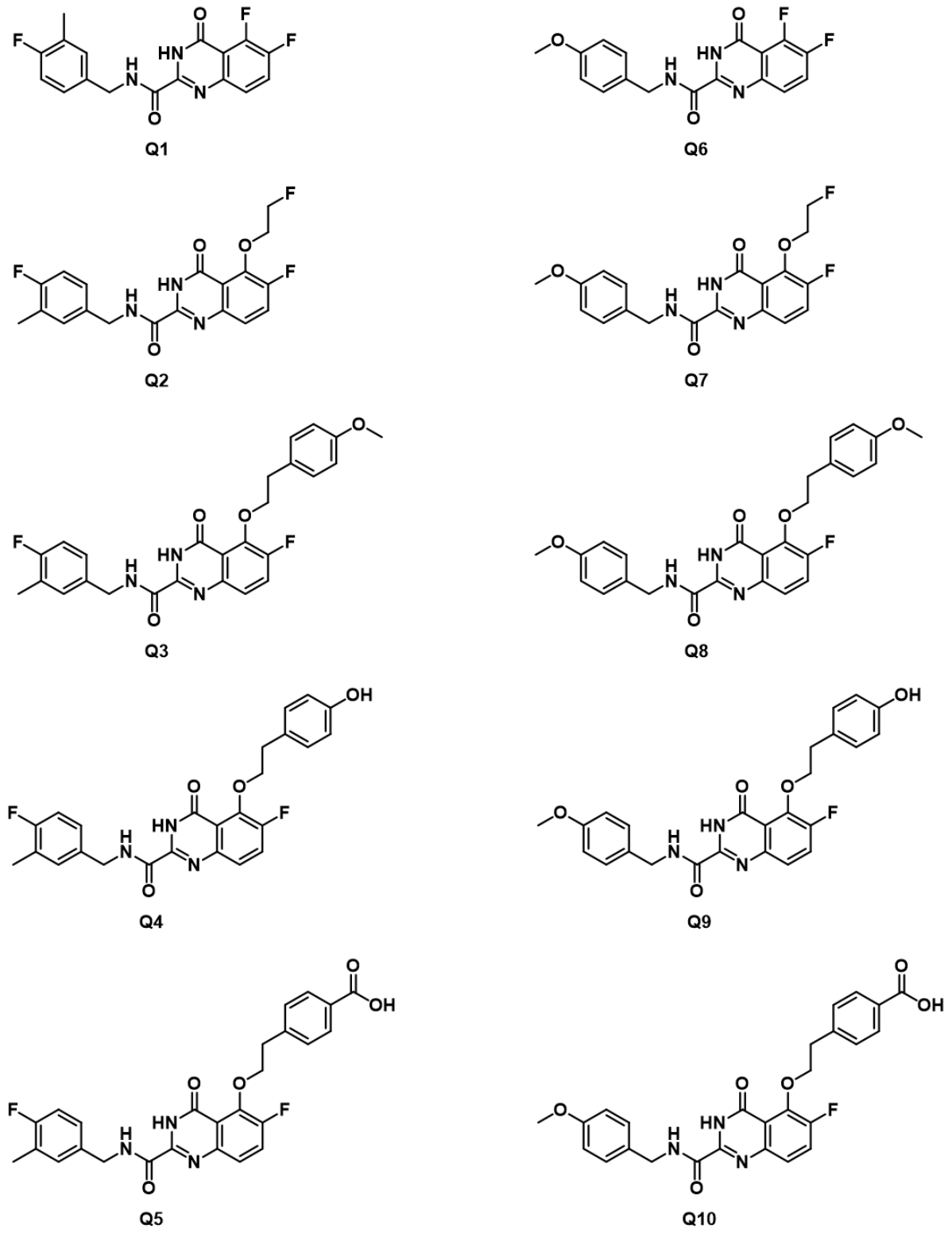

Figure 10: Chemical structures of Quinazoline core-based inhibitors.

This assay is run in an assay buffer: 50 mM Tris HCl, 10 mM $CaCl_2$,$2H_2O$, and 150 mM NaCl in distilled water. The pH of this solution is adjusted to 7.4 using concentrated NaOH. The enzymes are then activated using 4-aminophenylmercuric acetate (APMA), an organomercurial compound used to chelate zinc, disrupting the Cys-Zn^{2+} bond and freeing the pro-domain.[69] To activate the enzymes, 100 mM of APMA solution prepared in Dimethyl Sulfoxide (DMSO) by dissolving 176 mg of APMA in 5 ml of DMSO. Then, 500 µL of the APMA solution is added to 49.5 mL of assay buffer and mixed. To activate the MMPs, 10 µg of enzyme are first diluted in 100 µL to form 100 µg/mL concentrations of MMPs in APMA containing buffer. The mixture is then incubated at 37˚C for 2 hours. The activated MMPs are then diluted to 0.3 ng/mL in assay buffer. The substrate is also prepared in assay buffer as a 30 µM solution. The final assay conditions are 0.1 ng/mL of enzyme, 10 µM of substrate and different inhibitor concentrations prepared initially 3 times more concentrated than the final concentration. The general procedure for this assay is the following: the experiment is done in experimental triplicates using a black 96-well plate. For each triplicate, 2 nM of enzyme are incubated with different inhibitors concentrations ranging from 0.01 pM to 100 µM at 37ºC for 45 minutes. This was followed by the addition of 10 µM of substrate and the fluorescence was read for 15 minutes using Synergy HT fluorescent 96-well plate reader (λ excitation: 320 nm, λ emission: 405nm). Marimastat was used as a positive control, and a well containing enzyme and assay buffer was used as a negative control. After reading the fluorescence for each well in one minute intervals for 20 minutes, the relative fluorescence values (RFU) are plotted vs time (in minutes) using Graphpad prism, the slopes are generated using the software and percentage MMP activity is plotted vs log[inhibitor], assuming the values of the well containing the enzyme, substrate, and assay buffer as 100% enzyme activity, and the well with no enzyme (substrate and assay buffer only), a null enzyme activity. Previously, pyrimidine and quinazoline core inhibitors were used to synthesize inhibitors of MMPs.[51,53] The IC_{50}

values that were obtained using the previously described enzyme assay are comparable to the expected values obtained in previous studies.

The differences in the enzyme assay procedure between the different compounds tested was mainly the range of inhibitor concentrations adopted to generate an informative IC_{50} sigmoidal curve. More inhibitors are being synthesized at the moment and will also be tested for potency and selectivity using the previously described enzyme assay.

2.2 Radiofluorination

A series of chemical reactions are applied to eventually radiolabel the precursor P0 with fluoride-18 for upcoming *in vivo* and *ex vivo* studies. This is done to track the tracer using PET, quantify its biodistribution, in addition to colocalize the tracer with markers of inflammation.

The automated synthesis of fluorine-18-labelled P1 was developed by Ariel Buchler, a graduate student in our lab, and uses the GE FX2 N radiochemistry apparatus shown in figure 11 to develop the synthetic method which includes tracer synthesis, purification, and reformulation. This is the first inhibitor that was successfully radiolabeled following this scheme: fluorine-18 is strongly hydrated upon delivery, and deactivated towards nucleophilic reactions.[70] The fluorine-18 anion is purified from the aqueous environment to proceed with the fluorination chemistry. A quaternary ammonium ion exchange Sep-Pak column is used to purify fluorine-18. It uses quaternary ammonium bicarbonate salts that are replaced by the fluorine-18 anion.[70] Fluorine-18 is then eluted off the cartridge with potassium carbonate, and kryptofix is used to sequester potassium ions. Following fluorine drying, the precursor is added to the reaction vessel, and the reaction runs for 10 minutes at 140°C. It is then quenched and the whole content is transferred to the HPLC loop where it is purified and eluted with water followed by ethanol reformulation to make it suitable for animal studies (Figure 11).

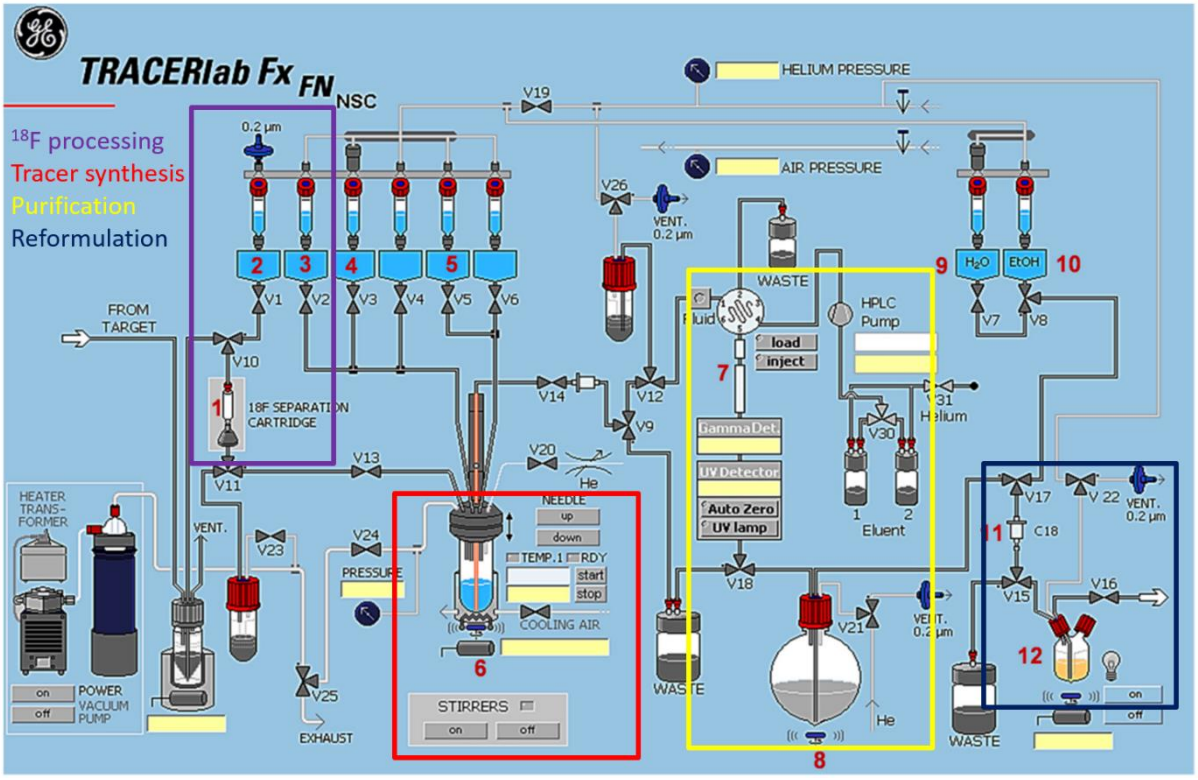

Figure 11: GE FX2 N radiochemistry apparatus used to radiolabel P0

Currently, an attempt to radiolabel inhibitor Q12 with carbon-11 is underway. This inhibitor was chosen due to its high potency and selectivity in inhibiting MMP-13 *in* vitro. In the future, more inhibitors will be labeled with fluorine-18 and carbon-11 to validate more potent tracers for testing in human studies.

2.3 Animal models

For the following *in vivo* and *ex vivo* studies, two groups of mice were used. The first consists of 4 months old healthy male C57Bl/6 mice on Normal Chow diet (NC), and the second group is 4 months old ApoE$^{-/-}$ male mice on 3 months Western diet (WD). A large number of calories are ingested in this form of diet. It consists mainly of refined carbohydrates

and cholesterol, as well as triglycerides. In addition, it is considered to be energy-dense but nutrient poor, and therefore, represents a risk factor for obesity, type 2 diabetes, and cardiovascular diseases.[71,72]

2.4 Autoradiography and blocking studies

Once the desired tracer is radiolabeled, its ability to bind to atherosclerotic plaque will be a further step into its validation. Furthermore, confirming that it is binding to the correct target (MMP-13) is important for its selectivity and specificity. This is tested in autoradiography blocking studies.

To determine tracer colocalization, en face aortas were harvested from the 2 groups of mice listed above. The aortas were placed on glass slides and pre-washed for 15 minutes in 50 nM Tris-HCl buffer (50 nM Tris HCl, 120 nM $NaCl_2$, 5 mM KCl, 1mM $MgCl_2$, 2 mM $CaCl_2$, pH 7.4, 25°C). For the blocking study, the aortas were incubated with an excess of cold standard (2 μM) at 25°C for 15 minutes to saturate specific binding sites, leaving only nonspecific binding. Then, they were washed with Tris-HCl before incubating both groups of aorta with 0.5 mCi/ mL of radiotracer (9nM) at 25°C for one hour. At the end of the incubation, the slides were washed for 2 x 10 minutes in fresh buffer at 4°C, washed once with deionized water at 4°C, and allowed to air dry in a fume hood for 20 minutes. While the slides were incubating, a set of serial dilutions was created using the radiotracer to convert the values from DLU/mm^2 to nCi/ml. 1 μl of each dilution was pipetted on a TLC plate. The phosphor screen was placed against a light box before use to erase background radiation. The slides and TLC plates were covered with plastic wrap and apposed to the phosphor screen in standard film cassettes for 20 hours. The screen was then scanned at 600 dpi resolution using a Cyclone storage phosphor system and the data was analyzed using Optiquant.

2.5 Tissue staining

In order to validate tracer colocalization in the plaque and better trace the boundaries of the atherosclerotic lesions, en face aortas obtained from both groups of mice were stained for high cholesterol content using oil red O. The main objective of this experiment was to test whether tracer uptake was indeed correlated with lesion localization. The en face aortas are covered with oil red O until the entire surface of the aorta is covered. The slides are then incubated for 50 minutes at room temperature. Then, oil red O is aspirated, and the aortas are excessively washed with distilled water before being photographed.

2.6 PET scans and biodistribution

Being able to dynamically track the radiolabeled tracer after tail vein injection is mice is essential in determining the sites of tracer binding and metabolism. Moreover, to evaluate the clearance characteristics of the radioligand, an *ex vivo* biodistribution study was performed.

PET experiments were carried out using a Siemens DPET microPET scanner. The images were acquired for 60 minutes and reconstructed unto dynamic time frames using a reconstruction algorithm. Mice are intravenously injected with 65-90 μCi of [^{18}F]P1 before being placed on the bed of the PET scanner and starting image acquisition. The PET images are also used in this case to determine the optimal time at which it is possible to see the tracer uptake in the aorta. Once this is determined, the same mice are injected again after a few days with the same dose of radiotracer, sacrificed at the proper time and tissues are collected, washed with PBS, and then placed in tubes for radioactivity measurement using the gamma counter. The tracer biodistribution results are acquired in counts per minute (CPM). A set of serial

dilutions is prepared to correspond each CPM value obtained from the gamma counter to Ci values.

2.7 Statistical analysis

Data for the enzyme assay plots, calibration curves, autoradiography studies and biodistribution assay are reported as mean + calculated error. Two-way analysis of variance followed by pairwise comparisons using Tukey correction was used to evaluate the treatment factor and treatment (C57Bl/6 vs $ApoE^{-/-}$ mice). Statistical analysis was performed using GraphPAD Prism Version 6.01 (La Jolla, CA). A $p < 0.05$ was considered statistically significant.

Chapter 3: Results and discussion

3.1 In vitro enzyme assay

The different IC_{50} of each compound synthesized in the lab based on the pyrimidine and quinazoline cores was compared with other IC_{50} with reference to Marimastat. This pan-MMP inhibitor had relatively close nanomolar range potencies vs all the MMPs tested with the lowest being 1.8 nM vs MMP-8 and the highest being 7.1 nM vs MMP-10. This small range of potencies between different MMPs is predicted since Marimastat acts on the Zn^{2+} present in all MMPs, so ne selectivity was expected to be observed in its potency.

The raw data is first obtained as RFU vs time (minutes) for 30 minutes. For each inhibitor concentration, an RFU value is recorded every minute, as shown in figure 12 for different concentrations of Marimastat. The numbers are then normalized for each inhibitor concentration by subtracting the RFU value at t = 0 minutes from each RFU value at the following time (figure 13). The slopes are then generated for each inhibitor concentration and plotted as a dose-response vs log of the concentration of the inhibitor used for the assay (figures 14 and 15). The IC_{50} values for Marimastat and all the tested inhibitors vs different MMPs are shown in table 3.

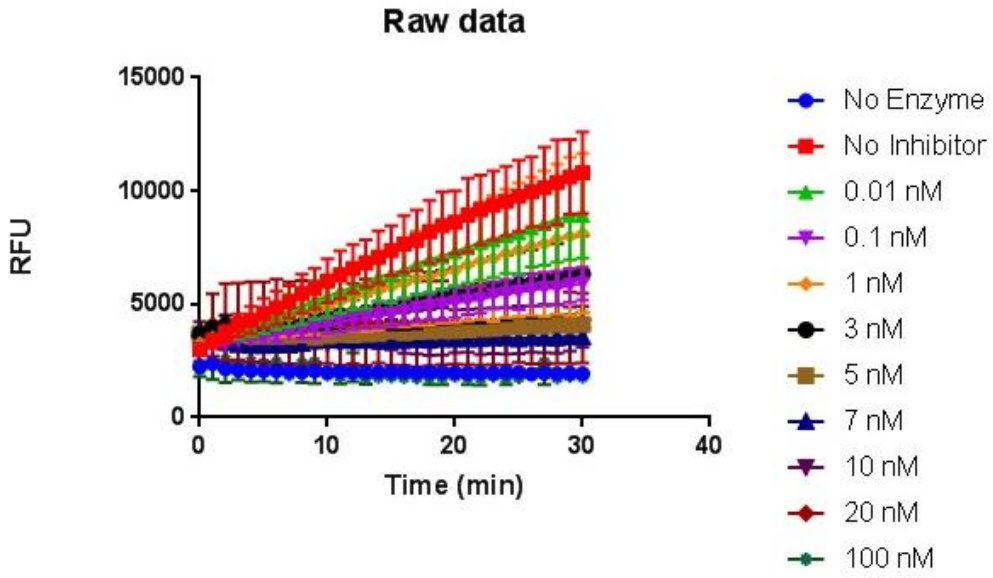

Figure 12: Raw data showing RFU vs time (min) for 30 minutes for Marimastat.

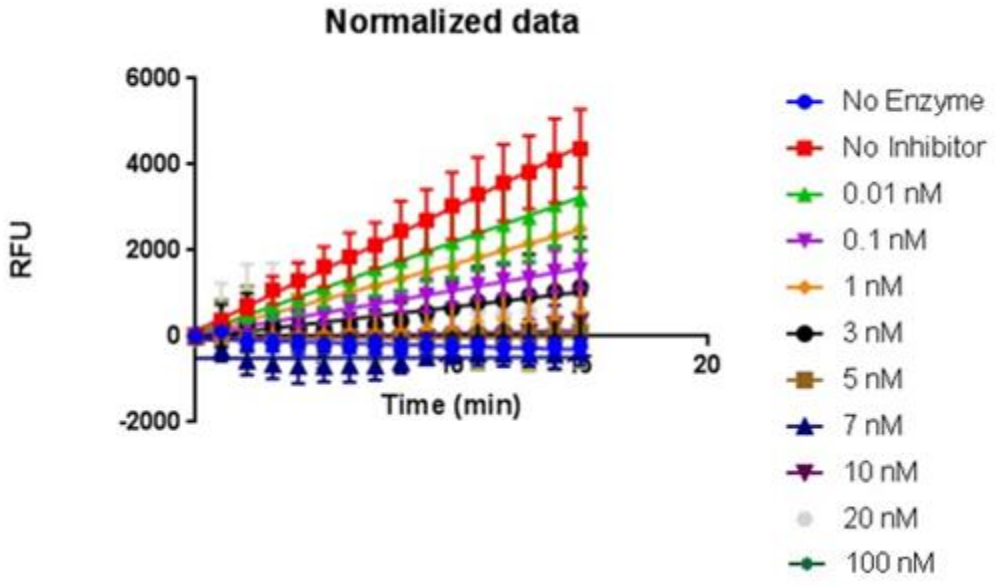

Figure 13: Normalized data showing RFU vs time (min) for 30 minutes for Marimastat.

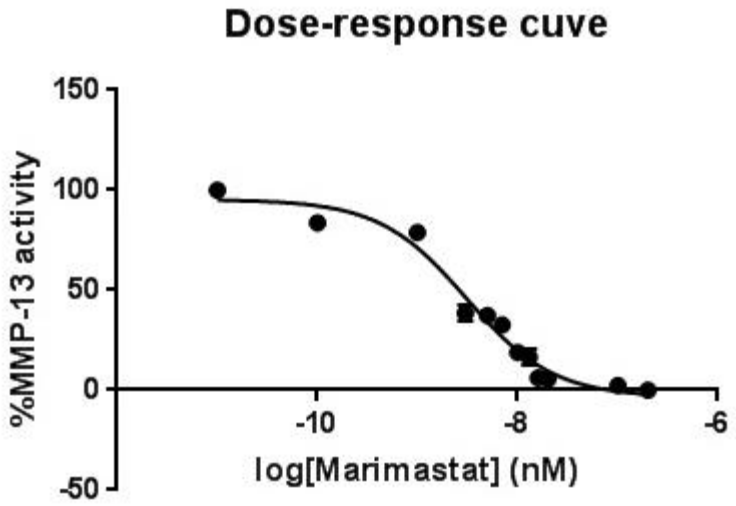

Figure 14: Dose response curve for Marimastat.

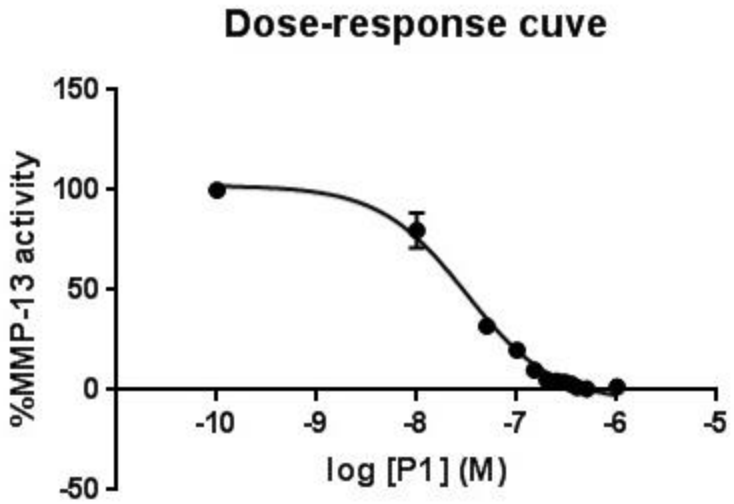

Figure 15: Dose response curve for inhibitor P1.

Compound		IC_{50} (nM)					
Name	Molecular weight g/mol	MMP-13	MMP-1	MMP-2	MMP-8	MMP-9	MMP-10
Marimastat	285.84	3.4	5	6	1.8	6.2	7.1
P1	440.45	33	>100	>100	96	98	83
P2	408.43	41	76	>100	51	>100	97
Q1	347.3	8.2	42	>100	45	26	3
Q2	391.35	4.1	38	>100	41	15	0.45
Q3	479.48	0.0039	36	>100	30	0.75	5
Q4	465.46	0.019	33	>100	28	8.5	20
Q5	493.47	0.0027	16	41	13	11	11
Q6	345.31	5.3	13	>100	34	9.4	6.2
Q7	389.36	2.6	>100	>100	>100	25	7.5
Q8	477.49	0.0072	19	>100	16	16	12
Q9	463.47	0.00123	14	>100	14	8.3	7.4
Q10	491.48	0.0048	12	48.9	22	13	9.1

Table 3: IC_{50} values of synthesized inhibitors vs MMP-1, -2, -8, -9, -10, -13

P1: Pyrimidine core inhibitor 1, P2: Pyrimidine core inhibitor 2,

Q2: Quinazoline core inhibitor 2, Q3: Quinazoline core inhibitor 3, Q4: Quinazoline core inhibitor 4, Q5: Quinazoline core inhibitor 5, Q6: Quinazoline core inhibitor 6, Q7: Quinazoline core inhibitor 7, Q8: Quinazoline core inhibitor 8, Q9: Quinazoline core inhibitor 9, Q10: Quinazoline core inhibitor 10.

The IC_{50} values in this table are shown in nanomolar. The >100 values represent IC_{50} values higher than 100 nM, ranging between 100 nM and 1.2 µM.

Similar patterns are observed between both derivatives of the pyrimidine core against different MMPs, with minor differences in potencies vs MMP-13. The replacement of the 2-fluoro-ethoxy group by the methoxy group does not seem to have a major effect on the potency when inspecting P1 and P2, and they are both less effective in inhibiting MMP-13 compared to Marimastat. However, one notable difference from Marimastat is the emerging of some selectivity towards MMP-13 in comparison to other MMPs. This is observable in this case by comparing the ratios between the IC_{50} values of MMP-13 vs MMP-2 and MMP-9. More differences in potencies and selectivity are observed in the next category of inhibitors based on

the quinazoline core. Q1, Q2, Q3, Q4, and Q5 share the same core, as well as the adjacent 4-fluoro-2-methyl-benzylamide group. However, each of these inhibitors has a different structure than the other. Q1 and Q2 have comparable potencies vs MMP-13 (8.2 nM and 4.1 nM respectively), as well as increased selectivity vs other MMPs, notably MMP-2, where the IC_{50} values were more than 100 nM. While the 2-fluoroethoxy group in Q2 seems to increase the potency compared to the fluorine in Q1, the next 3 inhibitors Q3, Q4 and Q5 are much more potent. These three compounds share a 2-methoxyethylbenzene moiety that seems to be an essential group in increasing potency. Q3 and Q5, with the methoxy and carboxylic acid groups, respectively, attached to the 2-mehtoxyethylbenzene moiety reach a potency of 0.0039 nM and 0.0027 nM, respectively, while Q4, with the hydroxy group, has a slightly lower potency of 0.019 nM. The next subcategory in the inhibitors based on the quinazoline core (Q6, Q7, Q8, Q9, Q10) share, in addition to the amide, a methoxybenzyl group instead of the 4-fluoro-2-methyl-benzylamide group. Compared to Q1 and Q2, which share the same variable groups directly attached to the quinazoline core, the 2-fluoroethoxy group and the fluorine atom, respectively, little difference is made by the methoxybenzyl group on the other side of the pyrimidine core: 5.3 nM and 2.6 nM for Q6 and Q7 compared to 4.1 nM and 8.2 nM in Q1 and Q2. The same pattern emerges upon addition of the substituted 2-mehtoxyethylbenzene moiety. Here, however, Q9, with the hydroxy group, seems to be more potent than Q8 and Q10, with IC_{50} values of 0.00123 nM for Q9 compared to 0.0072 nM and 0.0048 nM for Q8 and Q10, respectively. For the entire group of inhibitors based on the quinazoline core, higher degrees of selectivity are observed , in particular, compared to MMP-2 where the IC_{50} values are higher than 100 nM, with the exception of the highly MMP-13 potent Q5 and Q10. A certain degree of selectivity is also observed favoring MMP-13 over the remaining MMPs in all the other quinazoline inhibitors. Moreover, a certain pattern is present when comparing different quinazoline-based inhibitors. A small effect is seen when comparing the 2 different categories

of these inhibitors that differ in the nature of the group attached to the amide adjacent to the quinazoline core. Here, the differences are minimal, as seen in the IC_{50} values of compounds Q1 vs Q6, Q2 vs Q7, Q3 vs Q8, Q4 vs Q9, Q5 vs Q10, where the only structural difference between each pair of compounds is the group adjacent to the amide group attached to the quinazoline core. However, in the first category of quinazoline inhibitors, a greater difference is seen when the second position of the quinazoline fluorobenzene ring is replaced with the 2-mehtoxyethylbenzene moiety instead of the fluorine atom and the ethoxy fluorine group. The difference in the IC_{50} values upon addition of this moiety reached more than a 100-fold. The main advantage of this group, however, is due mainly to its large size, and occasionally to its hydrogen bond formations in the active site of the enzyme. As previously explained, upon docking of a large molecule on the S1' binding pocket, a second pocket known as the S1'* binding pocket opens up, allowing strong binding of the inhibitor. Therefore, this large moiety only represents an inhibitor molecular mass increase and an extension that helps the hydrogen binding groups to reach the S1'* binding pocket of MMPs. The results show that increasing molecular weights of the quinazoline core-based inhibitors contributes to the opening of the S1'* binding pocket. However, the hydrogen bonding to different lysine and threonine residues in this pocket is achieved by the groups added to the 2-mehtoxyethylbenzene moiety including the hydroxy group, the methoxy group and the carboxylic acid group. As for the cores of these molecules, the main difference seen can be due to the ability of the quinazoline core to establish more hydrogen bonds with the correspondent part of the enzyme compared to the pyrimidine core. No major changes in hydrogen binding are expected when replacing the group adjacent to the amide group and facing the S1' pocket. [38,51,52]

After comparing the IC_{50} values obtained through the *in vitro* enzyme assay done using all the available inhibitors and enzymes, it is noticeable that the pyrimidine-based inhibitors

are less potent than Marimastat, as well as all the quinazoline moieties. However, some degree of selectivity is achieved when comparing the potencies of P1 and P2 vs MMP-13 to all the other MMPs tested, notably, MMP-2 and MMP-9, which are of high importance. Even though the selectivity of these inhibitors for MMP-13 should be higher than all other MMPs, the gelatinases MMP-2 and MMP-9 are of additional importance, notably because both are shown to be increasingly expressed in the pathogenesis of the atherosclerotic plaque.[33,73] More specifically, it has been shown that atherogenesis is reduced in MMP-2-deficient ApoE$^{-/-}$ mice.[33,74] The mechanism by which this takes place is by blocking LDL cholesterol from being processed and penetrating the lumen of the vessels, trapping LDL in the bloodstream.[74] Moreover, in advanced plaque, where collagen I is present, MMP-2 is the main enzyme degrading this type collagen and involved in pathological vascular remodeling.[33] In addition, clinical studies suggest a role of MMP-2 in the stabilization of fibrous atherosclerotic plaques.[75] In another clinical study, MMP-2 is shown to be highly expressed in stable plaque compared to vulnerable ones.[76] Consequently, inhibiting MMP-2 can promotes the progression of atherosclerotic plaques, as well as the vulnerability of the fibrous cap. On the other hand, although it has been shown that MMP-9 is present in large quantities in atherosclerotic plaques, and upregulation of this enzyme is directly correlated with increase of atherosclerotic plaque hemorrhage and rupture it has also been shown that the deletion of MMP-9 is associated with plaque development, suggesting a beneficial role of MMP-9 in the prevention of atherosclerotic plaque progression.[33,73,77] Therefore, due to the different effects of MMP-9 in different stages of atherosclerosis, it is best to avoid any interaction of the inhibitors with this enzyme. As for the other MMPs tested, MMP-8 is known to be an activator of other MMPs, mainly MMP-2 and MMP-9, and MMP-10, are not highly present in atherosclerotic plaques compared to the others, but are more structurally similar to MMP-13. [73,77,78]

In summary, it has been noticed that the scaffold bound to the fluorobenzene ring on the right of the quinazoline core is making the inhibitors more potent in general. This is due to the interaction between the carboxylic acid and the nitrogen hydrogen on the Lys140 in the S1'* binding pocket, thereby, strengthening the interaction between the inhibitor and the enzyme. Therefore, the main target for future syntheses is the addition of functional groups that will reach and bind to more residues in the S1'* pocket to reach a high level of potency and design an inhibitor that only binds and inhibits MMP-13.

3.2 Radiofluorination

The radiofluorination of P0 shown in figure 16 was successful and produced [^{18}F]P1with a decay corrected yield of 29%, a molar activity of 2.55 Ci/µmol, and radiochemical purity more than 99%. The whole reaction took 62 minutes, which is a suitable time with respect to the half-life of fluorine-18. The tracer was reformulated in 0.9% NaCl, making it suitable for animal injection. This method of radiofluorination can be also altered to be used with other inhibitors.

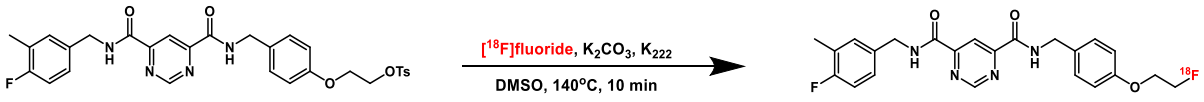

Figure 16: General synthesis scheme for the automated synthesis of [^{18}F] labeled inhibitor P1

3.3 Autoradiography and blocking studies

In order to colocalize tracer uptake in atherosclerotic lesions, the radiolabelled inhibitor P1 was tested for potential atherosclerotic plaque binding. After incubating the en face aortas

overnight with the phosphor screen, the image was generated, and an example of the acquired results is shown in figure 17.

These images of the aorta show a difference in uptake between C57Bl/6 mice and $ApoE^{-/-}$ mice on Western diet, notably on the edge of the aortic arch. When comparing the baseline uptake with the blocking uptake, the C57Bl/6 aortas show higher washout than the $ApoE^{-/-}$. These results are replicated in n = 4 of each group, showed in figure 17. The relative light units (DLU) acquired initially from the Cyclon storage software system (Optiquant) were converted to percentage of incubation dose (%ID) using a calibration curve shown in figure 18, where lesions were selected. %ID is calculated by dividing the quantification of the activity (either in DLU or nCi/ml) measured in a lesion over the entire activity present on the whole aorta, then multiplied by 100. Ideally, the expectations from this study were to see a more significant decreased binding in blocking experiments: in particular, the difference between the baseline and blocking studies in the $ApoE^{-/-}$ mice should have been higher than the one in C57Bl/6 mice. Moreover, the uptake in C57Bl/6 baseline model seems to be significant, which may be due to the lack of target specificity of inhibitor P1. This is confirmed by the measured uptake in the arch. Indeed, this is shown in the enzyme assay, when comparing P1 to other inhibitors. This drawback can be overcome by developing a more efficient method for homogenous incubation of the aortas with the tracer. In the future, this experiment will undergo optimization, starting with the determination of the optimal incubation times and tracer concentrations using different longitudinal studies. This also requires an adjustment of the exposure time of the aortas to the phosphor screen to also determine the optimal exposure time and avoid screen saturation. In addition, non-specific binding can be avoided when the aortas are washed with bovine serum albumin (BSA) and washed more extensively with PBS. By using BSA, the proteins are blocked and are therefore unlikely to interact with any random moiety that does not show high selectivity towards a specific protein. In our example, only

proteins that selectively interact with our tracer will bind to it. This will decrease background noise and unspecific binding. Therefore, strong and selective interactions between our tracers and MMP-13 are necessary to ensure a proper validation of the selectivity of the tracers towards this enzyme compared to other targets. Consequently, more potent radiolabeled inhibitors can be used to achieve better and more conclusive autoradiography results. Furthermore, target density can be measured using the cold standard (P0) as a block, and more specificity targeted studies can be done by using Marimastat, or another pan MMP inhibitor as a block. By using pan MMP inhibitors as blocking agents, the selectivity of the inhibitor is gradually narrowed down: pan inhibitors block all MMPs from binding to any target, therefore, a decrease in the signal compared to baseline studies indicates that the tested tracer is actually binding to an MMP. Finally, selectivity studies become more feasible when using a validated commercially available highly potent MMP-13 inhibitor. Following optimization, this study can be repeated using an 8 months old cohort on western diet for 5-6 months to ensure advanced lesion development.

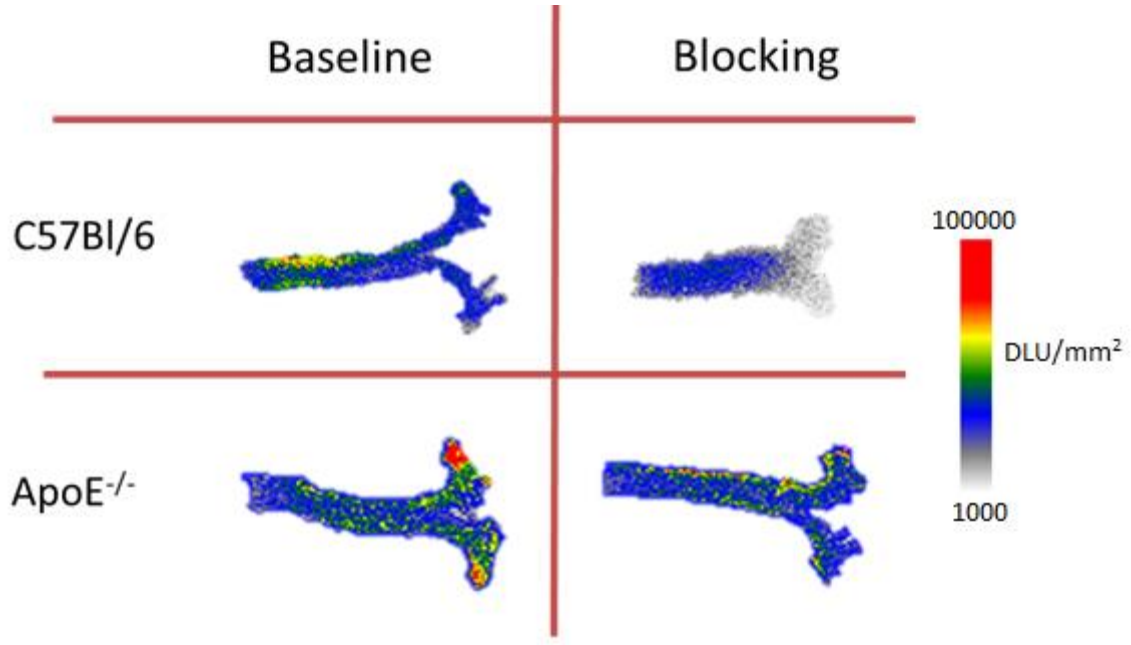

Figure 17: Different uptake patterns in baseline and blocking studies done on C57Bl/6 mice and ApoE$^{-/-}$ mice on Western diet.

The aortas from the 2 baseline groups were incubated with 9 nM of the tracer. The aortas from the blocking studies were preincubated with 2 μM of the non radiolabelled tracer. The aortas were exposed overnight to a phosphor screen.

The scale on the right side of the image shows the intensity of the dose on the phosphor screen.

The red color indicates higher decay, directly correlated with higher tracer concentrations.

The blue and grey colors indicate lower decay, directly correlated with lower tracer concentrations.

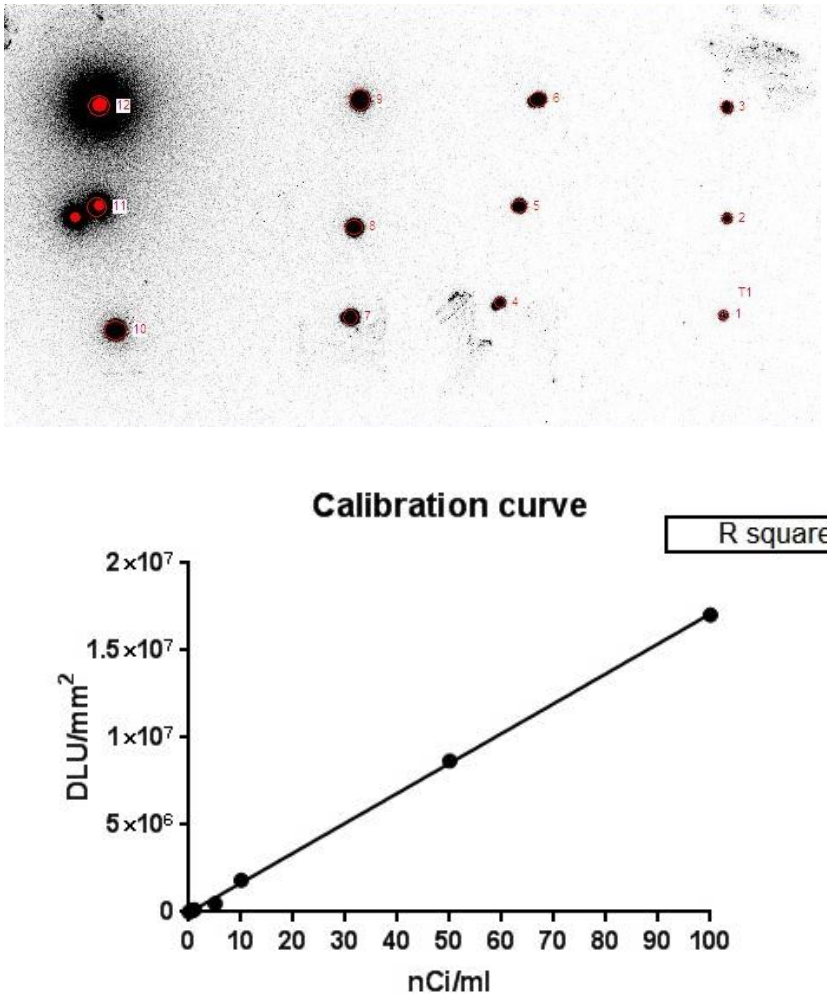

Figure 18: Autoradiogram and its corresponding calibration curve used to convert DLU/mm^2 values to nCi/ml.

1 μl of a each concentration of set of serial dilutions of the radiolabelled tracer were dropped on the TLC plate which was then exposed to the phosphor screen overnight along with the aortas. The calibration curve was used to better quantify activity uptake to get comparable units to the ones in the literature.

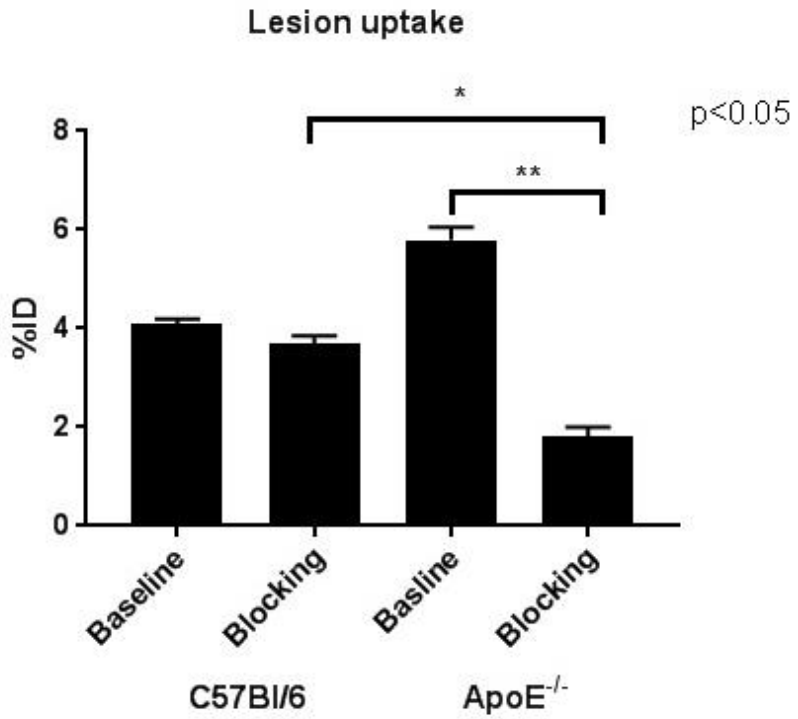

Figure 19: Measurement of uptake in %ID in the different groups of mice (n = 4).

Autoradiograms were obtained for baseline and blocked aortas from the 2 groups of mice. The uptake in the arch was then quantified in %ID for each aorta and divided by the uptake of the whole aorta. More washout is observed when comparing the baseline and blocking data of the ApoE $^{-/-}$ mice than the one seen in the C57Bl/6 mice. Also, a large difference in uptake was observed between the blocking group of the 2 groups. %ID: percentage of incubation dose of [^{18}F]P1 .

3.4 Tissue staining

A location similarity is seen between the sites of tracer uptake shown by autoradiography and the sites of high oil red O staining in the aortas of both groups of mice (Figure 20). This is a preliminary indication of the tracer binding to the sites of high lipid and triglycerides content, a characteristic of atherosclerotic lesions.

More studies need to be done to confirm valid tracer binding sites. These include immunohistochemistry techniques using anti-CD-68 antibodies to correlate tracer uptake with markers of inflammation. These studies also showed a difficulty in staining en face aortas; sectioning the lesioned aortas into 10 µm sections might be the way to go forward for CD-68 immunostaining. In addition, to confirm that the radiolabeled inhibitors are binding to MMP-13 selectively, antibodies can be radiolabeled with iodine-125 and the en face aorta can be imaged using autoradiography. For this experiment, autoradiography studies using the radiolabeled tracers should be preferably done prior to incubation to antibodies, due to the strong interaction between antibodies and their targets. Following radiotracer incubation, the images are acquired, and the aortas are washed extensively with PBS, then incubated with BSA. Subsequently, the aortas are incubated with appropriate concentrations of iodine-125-labeled anti-MMP-13 antibodies. After adequate incubation duration, the aortas are exposed to the phosphor screen again and after a certain time, the images are acquired and are overlaid with the tracer autoradiographs. Colocalization is then a strong evidence that the tracer is selectively binding to MMP-13. Due to the selectivity of antibodies to their moieties, they can be an advanced marker for validation of the tracers. In addition, antibodies are relatively easy to label with radioiodine and other radiometals.[79]

(A)

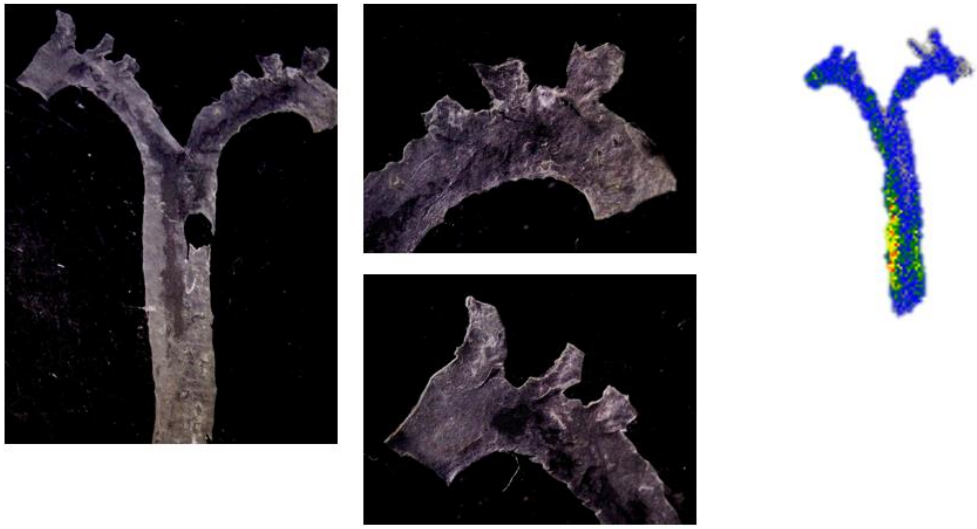

(B)

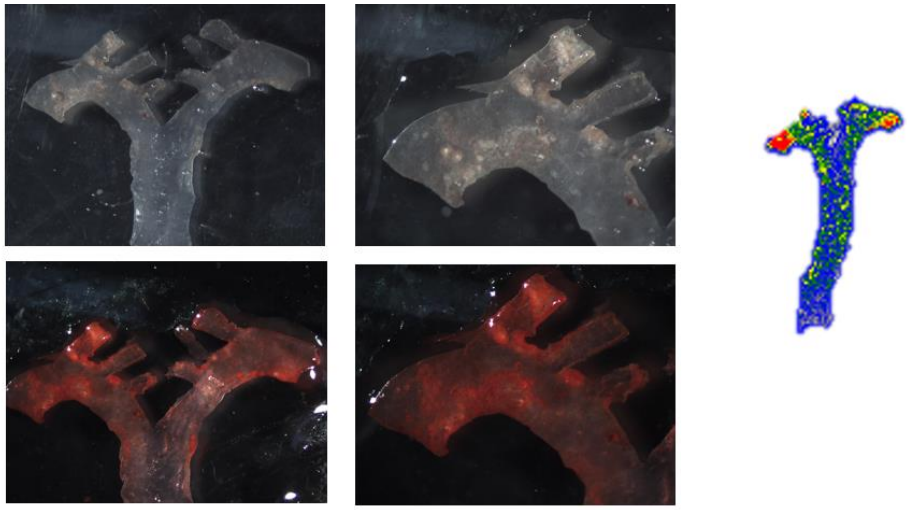

Figure 20: Tissue staining of harvested en-face aorta. (A): oil red O image of the en face aorta of a C57Bl/6 mouse with the autoradiography image. (B): oil red O image of the en face aorta of an ApoE$^{-/-}$ mouse with the autoradiography image. Oil red O images of ApoE$^{-/-}$ mice show regions of high lipid content that can be correlated with the autoradiogram.

3.5 PET scans and biodistribution

Representative coronal whole-body images 20-30 min after tracer injection are shown in figure 21. While these images show comparable uptake in the liver and heart in this time interval, it is almost impossible to locate the aorta due to the strong signal originating for the liver and the heart in these images. However, these scans were useful in determining the exact moment where the heart uptake is the highest. Moreover, time activity curves were plotted for these PET scans (figure 22). The uptake is the highest at 3-5 minutes, followed by fast clearance of the radiotracers. Both groups show a low heart retention and a fast clearance indicating the low amount of target in the heart, thereby reducing background noise.

Also, to evaluate the clearance characteristics of the radioligand [^{18}F]P1, an *ex vivo* biodistribution study was performed with both mouse models used before. The time point selected for euthanasia was based on the PET scans done previously, based on the time activity curve shown in figure 22. We determined that 20-25 minutes post injection was a suitable time for sacrificing the mice and harvesting their organs due to the signal washout observed during these timepoints. To data collected from the γ-counter are in CPM. The calibration curve shown in figure was used to convert these values into μCi/ ml. The biodistribution data confirms the PET data as the uptake of the tracer is the largest in the liver at this time points where the mice were sacrificed. This is shown in figure 24.

Even though these methods have been efficient in showing dynamic tracer uptake in different organs of the mice, imaging an en face aorta using PET and getting its total tracer uptake using the gamma counter is another way to measure uptake. This can also be coupled with blocking studies *in vivo* where a signal washout will be an important outcome, indicating an identical behavior of the tracer *in vivo* and *ex vivo*. As for the biodistribution assays, no

significant changes are expected, since the inhibitor is similarly metabolized in both groups of mice. However, another more efficient way of checking for tracer metabolism is performing metabolite studies on both groups of mice.

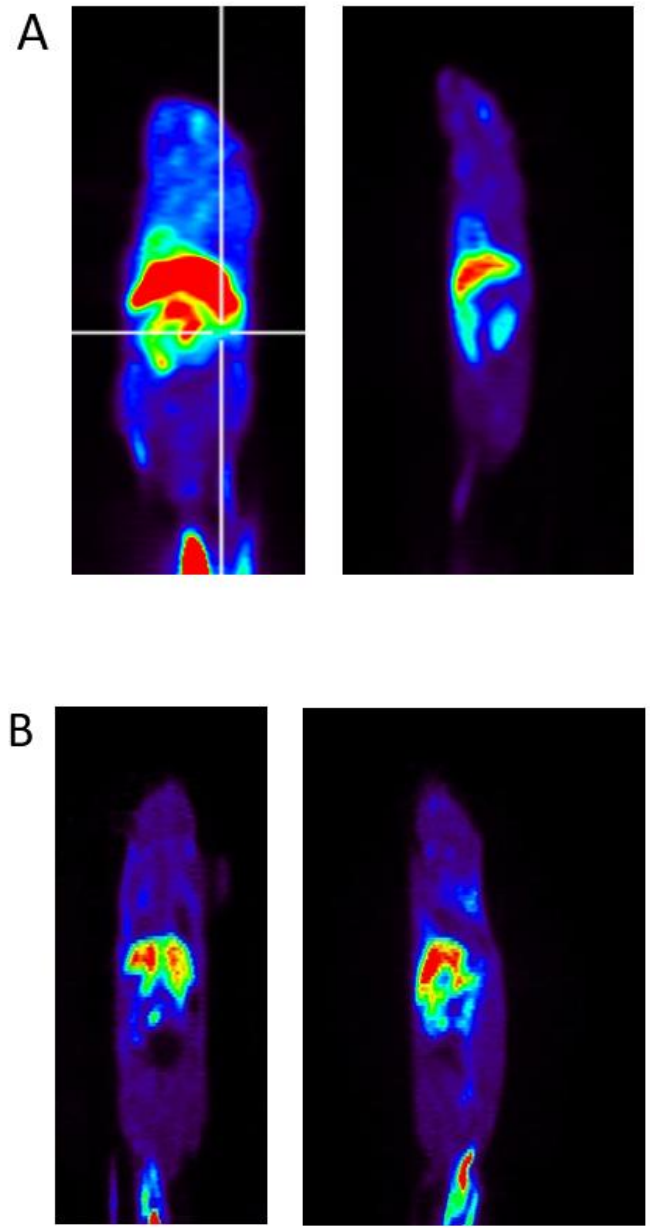

Figure 21: Coronal whole-body images of C57Bl/6 mice (A) and ApoE$^{-/-}$ mice (B).

Mice were intravenously injected with 65-90 µCi of radiotracer and the images were acquired for 60 minutes. The images show similar patterns of uptake indicating an identical distribution of the tracer in the 2 groups of mice.

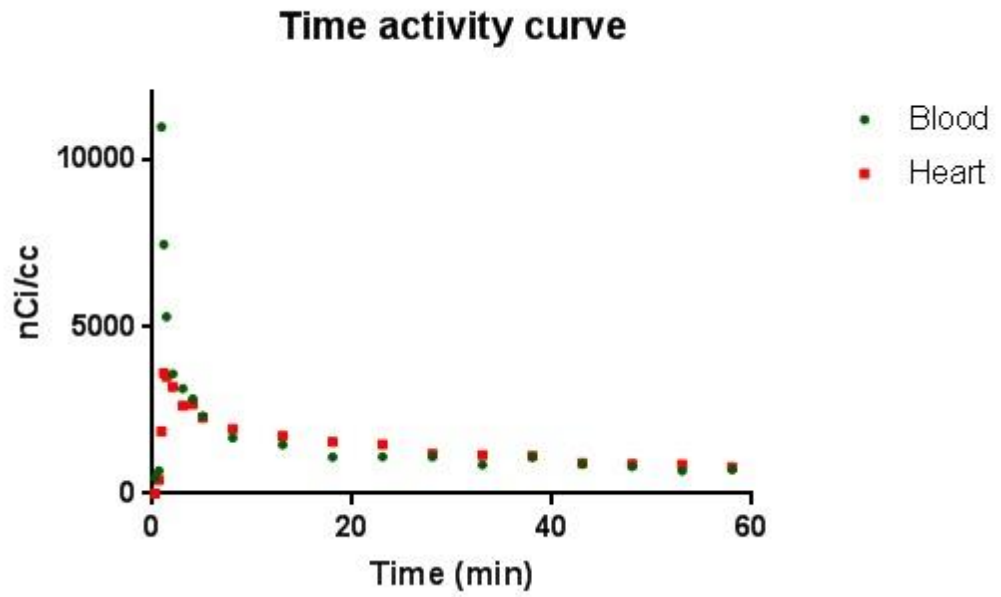

Figure 22: Time activity curve showing blood and whole heart tracer uptake.

The time activity curves for each organ were obtained by selecting a region of interest (ROI) around the organ. The heart ROI was taken from the left ventricle wall, and blood ROI was taken from the blood inside the left ventricle.

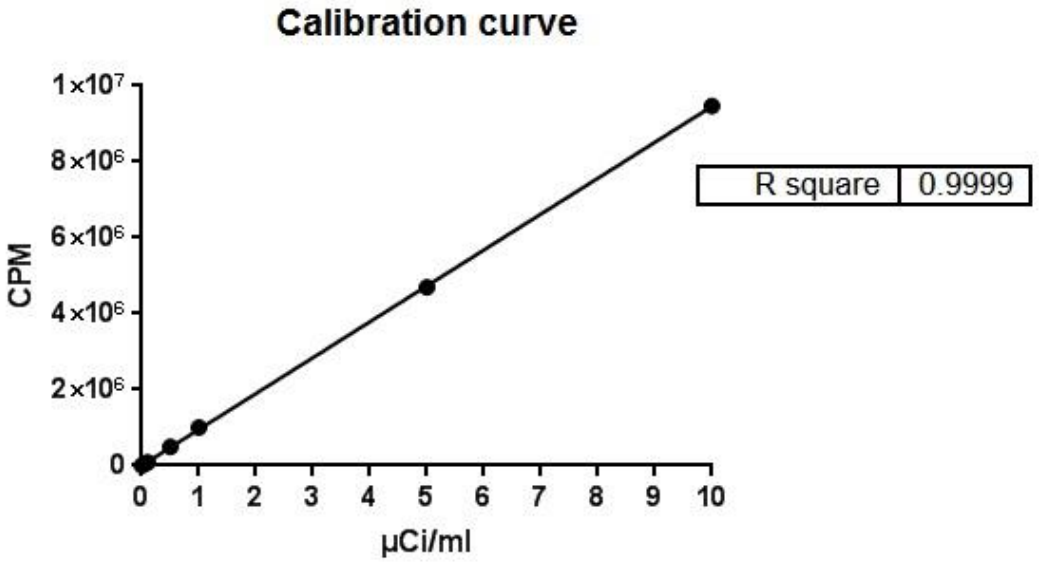

Figure 23: Calibration curve used to convert CPM values to µCi/ml.

1 ml of each concentration of set of serial dilutions of the radiolabelled tracer were placed in counting tubes and their counts were read by the gamma counter before counting the activity in the harvested organs. The calibration curve was used to better quantify activity uptake to get comparable units to the ones in the literature.

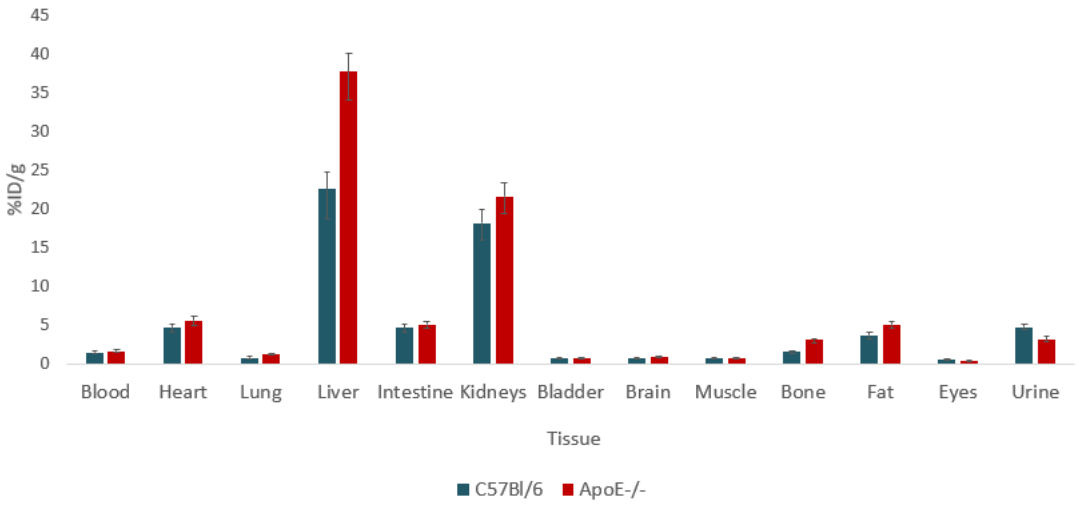

Figure 24: *ex vivo* biodistribution of [^{18}F]Inhibitor P1 in control vs ApoE$^{-/-}$ mice. (n= 3).

The mice were sacrificed at 20-25 minutes post injection and some of the essential organs were harvested, washed with PBS, and counted for one minute using the gamma counter. The results show a similar distribution of the tracer in the 2 groups of mice tested indicating a similar metabolism of the tracer in the body.

Chapter 4: Conclusion

In summary, among all the inhibitors tested using the enzyme assay described earlier, the group that is making the inhibitors more potent is the scaffold bound to the fluorobenzene ring on the right of the quinazoline core. Moreover, the radiofluorination of P0 was successful and produced [^{18}F]P1 and this inhibitor was used in *in vivo* experiments. In addition, oil red O staining and colocalization studies using [^{18}F]P1 showed target specificity indicating that the tracer is binding to regions of high lipid content. More experiments are needed to be done in order to validate whether this inhibitor is only binding to MMP-13. Finally, PET scans and biodistribution studies showed similar behavior of the tracer *in vivo.*

Although [^{18}F]P1 was promising in this research, it was not very potent against MMP-13. In addition, some limitations were faced while running colocalization studies: these include small lesions in ApoE$^{-/-}$ mice, unspecific binding, unequal washing, and others. Many optimizations are needed to ultimately develop the most potent and selective MMP-13 inhibitor for atherosclerosis.

The main target for future syntheses is the addition of functional groups that can bind to the S1'* pocket to reach a high level of potency and design an MMP-13 selective inhibitor. Moreover, selectivity studies would be more conclusive when using a validated selective MMP-13 inhibitor. Also, an older cohort can be placed on western diet for 5-6 months to ensure advanced lesion development. In addition, metabolite studies can be performed in order to better assess the metabolism of the tracer in mice.

In conclusion, this work showed that a wide scope of inhibitors can be synthesized to selectively inhibit MMP-13. Also, radiofluorination of the selected inhibitor was successful for animal studies. Moreover, en face aorta autoradiography was successful and the results are

promising for future inhibitors. In addition, even one of the least potent tracers was efficient in targeting atherosclerotic plaques. More methods need to be developed and a way to observe aortic uptake using PET scans can be very helpful.

.

Chapter 5. References

1. Al-Haddad, R., Ismailani, U. S. & Rotstein, B. H. Current and Future Cardiovascular PET Radiopharmaceuticals. *PET Clin* **14**, 293–305 (2019).

2. Mensah, G. A. & Brown, D. W. An overview of cardiovascular disease burden in the United States. *Health Aff (Millwood)* **26**, 38–48 (2007).

3. The top 10 causes of death. *World Health Organization* http://www.who.int/news-room/fact-sheets/detail/the-top-10-causes-of-death.

4. Stewart, J., Manmathan, G. & Wilkinson, P. Primary prevention of cardiovascular disease: A review of contemporary guidance and literature. *JRSM Cardiovasc Dis* **6**, 2048004016687211 (2017).

5. Cassar, A., Holmes, D. R., Rihal, C. S. & Gersh, B. J. Chronic coronary artery disease: diagnosis and management. *Mayo Clin. Proc.* **84**, 1130–1146 (2009).

6. WHO | Disease burden and mortality estimates. *WHO* http://www.who.int/healthinfo/global_burden_disease/estimates/en/.

7. Mozaffarian, D. *et al.* Heart disease and stroke statistics--2015 update: a report from the American Heart Association. *Circulation* **131**, e29-322 (2015).

8. Blumgart, H. L. & Weiss, S. STUDIES ON THE VELOCITY OF BLOOD FLOW. *J Clin Invest* **4**, 399–425 (1927).

9. Prinzmetal, M., Corday, E., Bergman, H. C., Schwartz, L. & Spritzler, R. J. Radiocardiography: A New Method for Studying the Blood Flow Through the Chambers of the Heart in Human Beings. *Science* **108**, 340–341 (1948).

10. Slomka, P. J. *et al.* Cardiac imaging: working towards fully-automated machine analysis & interpretation. *Expert Rev Med Devices* **14**, 197–212 (2017).

11. Berger, A. Positron emission tomography. *BMJ* **326**, 1449 (2003).

12. Vaquero, J. J. & Kinahan, P. Positron Emission Tomography: Current Challenges and Opportunities for Technological Advances in Clinical and Preclinical Imaging Systems. *Annu Rev Biomed Eng* **17**, 385–414 (2015).

13. Lameka, K., Farwell, M. D. & Ichise, M. Positron Emission Tomography. *Handb Clin Neurol* **135**, 209–227 (2016).

14. Zhu, A., Lee, D. & Shim, H. Metabolic PET Imaging in Cancer Detection and Therapy Response. *Semin Oncol* **38**, 55–69 (2011).

15. Chouinard, J. A., Rousseau, J. A., Beaudoin, J.-F., Vermette, P. & Lecomte, R. Positron emission tomography detection of human endothelial cell and fibroblast monolayers: effect of pretreament and cell density on 18FDG uptake. *Vasc Cell* **4**, 5 (2012).

16. Miele, E. *et al.* Positron Emission Tomography (PET) radiotracers in oncology – utility of 18F-Fluoro-deoxy-glucose (FDG)-PET in the management of patients with non-small-cell lung cancer (NSCLC). *J Exp Clin Cancer Res* **27**, 52 (2008).

17. Li, Y., Zhang, W., Wu, H. & Liu, G. Advanced Tracers in PET Imaging of Cardiovascular Disease. *BioMed Research International* **2014**, 1–13 (2014).

18. Conti, M. & Eriksson, L. Physics of pure and non-pure positron emitters for PET: a review and a discussion. *EJNMMI Physics* **3**, (2016).

19. Lusis, A. J. Atherosclerosis. *Nature* **407**, 233 (2000).

20. Rafieian-Kopaei, M., Setorki, M., Doudi, M., Baradaran, A. & Nasri, H. Atherosclerosis: Process, Indicators, Risk Factors and New Hopes. *Int J Prev Med* **5**, 927–946 (2014).

21. Riccioni, G. *et al.* Atherosclerotic Plaque Formation and Risk Factors. *Int J Immunopathol Pharmacol* **16**, 25–31 (2003).

22. Rodondi, N. *et al.* Markers of atherosclerosis and inflammation for prediction of coronary heart disease in older adults. *Am. J. Epidemiol.* **171**, 540–549 (2010).

23. Suzuki, H. *et al.* A role for macrophage scavenger receptors in atherosclerosis and susceptibility to infection. *Nature* **386**, 292–296 (1997).

24. Finn Aloke V., Nakano Masataka, Narula Jagat, Kolodgie Frank D. & Virmani Renu. Concept of Vulnerable/Unstable Plaque. *Arteriosclerosis, Thrombosis, and Vascular Biology* **30**, 1282–1292 (2010).

25. Bergheanu, S. C., Bodde, M. C. & Jukema, J. W. Pathophysiology and treatment of atherosclerosis. *Neth Heart J* **25**, 231–242 (2017).

26. Della Rocca, D. G. & Pepine, C. J. Endothelium as a Predictor of Adverse Outcomes: Endothelium as a predictor of adverse outcomes. *Clinical Cardiology* **33**, 730–732 (2010).

27. Bode Michaela K. *et al.* Complete Processing of Type III Collagen in Atherosclerotic Plaques. *Arteriosclerosis, Thrombosis, and Vascular Biology* **19**, 1506–1511 (1999).

28. Lodish, H. *et al.* Collagen: The Fibrous Proteins of the Matrix. *Molecular Cell Biology. 4th edition* (2000).

29. Shiomi, M., Ito, T., Hirouchi, Y. & Enomoto, M. Fibromuscular cap composition is important for the stability of established atherosclerotic plaques in mature WHHL rabbits treated with statins. *Atherosclerosis* **157**, 75–84 (2001).

30. Bentzon Jacob Fog, Otsuka Fumiyuki, Virmani Renu & Falk Erling. Mechanisms of Plaque Formation and Rupture. *Circulation Research* **114**, 1852–1866 (2014).

31. Rekhter, M. D. Collagen synthesis in atherosclerosis: too much and not enough. *Cardiovasc Res* **41**, 376–384 (1999).

32. Adiguzel, E., Ahmad, P. J., Franco, C. & Bendeck, M. P. Collagens in the progression and complications of atherosclerosis. *Vascular Medicine* **14**, 73–89 (2009).

33. Vacek, T. P. *et al.* Matrix metalloproteinases in atherosclerosis: role of nitric oxide, hydrogen sulfide, homocysteine, and polymorphisms. *Vasc Health Risk Manag* **11**, 173–183 (2015).

34. Newby, A. C. Metalloproteinases promote plaque rupture and myocardial infarction: A persuasive concept waiting for clinical translation. *Matrix Biol.* **44–46**, 157–166 (2015).

35. Spinale, F. G. Matrix metalloproteinases: regulation and dysregulation in the failing heart. *Circ. Res.* **90**, 520–530 (2002).

36. Ricard-Blum, S. The Collagen Family. *Cold Spring Harb Perspect Biol* **3**, (2011).

37. Hrabec, E., Naduk, J., Strek, M. & Hrabec, Z. [Type IV collagenases (MMP-2 and MMP-9) and their substrates--intracellular proteins, hormones, cytokines, chemokines and their receptors]. *Postepy Biochem.* **53**, 37–45 (2007).

38. Nagase, H., Visse, R. & Murphy, G. Structure and function of matrix metalloproteinases and TIMPs. *Cardiovasc Res* **69**, 562–573 (2006).

39. Av, P., Da, K., Va, K., Av, G. & An, O. Metalloproteinases, Sialidases and NADPH Oxidases as Key Enzymes involved in Atherosclerosis Development. *Archives of Clinical Microbiology* 6 (2019).

40. Newby, A. C. Metalloproteinases and Vulnerable Atherosclerotic Plaques. *Trends Cardiovasc Med* **17**, 253–258 (2007).

41. Lemaître, V. *et al.* ApoE knockout mice expressing human matrix metalloproteinase-1 in macrophages have less advanced atherosclerosis. *J. Clin. Invest.* **107**, 1227–1234 (2001).

42. Newby, A. C. Matrix metalloproteinases regulate migration, proliferation, and death of vascular smooth muscle cells by degrading matrix and non-matrix substrates. *Cardiovasc. Res.* **69**, 614–624 (2006).

43. Johnson, J. L., George, S. J., Newby, A. C. & Jackson, C. L. Divergent effects of matrix metalloproteinases 3, 7, 9, and 12 on atherosclerotic plaque stability in mouse brachiocephalic arteries. *PNAS* **102**, 15575–15580 (2005).

44. Silence, J., Lupu, F., Collen, D. & Lijnen, H. R. Persistence of atherosclerotic plaque but reduced aneurysm formation in mice with stromelysin-1 (MMP-3) gene inactivation. *Arterioscler. Thromb. Vasc. Biol.* **21**, 1440–1445 (2001).

45. Fukumoto, Y. *et al.* Genetically determined resistance to collagenase action augments interstitial collagen accumulation in atherosclerotic plaques. *Circulation* **110**, 1953–1959 (2004).

46. Deguchi, J.-O. *et al.* Matrix metalloproteinase-13/collagenase-3 deletion promotes collagen accumulation and organization in mouse atherosclerotic plaques. *Circulation* **112**, 2708–2715 (2005).

47. Quillard, T. *et al.* Selective inhibition of matrix metalloproteinase 13 (MMP-13) increases collagen content of established mouse atheromata. *Arterioscler Thromb Vasc Biol* **31**, 2464–2472 (2011).

48. Jabłońska-Trypuć, A., Matejczyk, M. & Rosochacki, S. Matrix metalloproteinases (MMPs), the main extracellular matrix (ECM) enzymes in collagen degradation, as a target for anticancer drugs. *Journal of Enzyme Inhibition and Medicinal Chemistry* **31**, 177–183 (2016).

49. Gomis-Rüth, F. X. Structural aspects of the metzincin clan of metalloendopeptidases. *Mol. Biotechnol.* **24**, 157–202 (2003).

50. Snoek-van Beurden, P. A. M. & Von den Hoff, J. W. Zymographic techniques for the analysis of matrix metalloproteinases and their inhibitors. *BioTechniques* **38**, 73–83 (2005).

51. Hugenberg, V. *et al.* Radiolabeled Selective Matrix Metalloproteinase 13 (MMP-13) Inhibitors: (Radio)Syntheses and in Vitro and First in Vivo Evaluation. *J. Med. Chem.* **60**, 307–321 (2017).

52. Li, J. J. & Johnson, A. R. Selective MMP13 inhibitors. *Med Res Rev* **31**, 863–894 (2011).

53. Nara, H. *et al.* Discovery of Novel, Highly Potent, and Selective Quinazoline-2-carboxamide-Based Matrix Metalloproteinase (MMP)-13 Inhibitors without a Zinc Binding Group Using a Structure-Based Design Approach. *J. Med. Chem.* **57**, 8886–8902 (2014).

54. Bardhan, K. D., Cullis, J., Williams, N. R., Arasaradnam, R. P. & Wilson, A. J. Quantification of 18FDG in the Normal Colon—A First Step in Investigating Whether Its Presence Is a Marker of a Physiological Process. *PLOS ONE* **11**, e0147838 (2016).

55. Cocker, M. S. *et al.* [18F]-Fluorodeoxyglucose PET/CT imaging as a marker of carotid plaque inflammation: Comparison to immunohistology and relationship to acuity of events. *International Journal of Cardiology* **271**, 378–386 (2018).

56. Belhocine, T. *et al.* 18FDG PET in oncology: the best and the worst (Review). *Int. J. Oncol.* **28**, 1249–1261 (2006).

57. Wakabayashi, H. *et al.* Focal 18F-FDG Uptake in Acute inflammation is Associated with CD68-Positive Macrophage Infiltration in a Rat Model of Autoimmune Myocarditis. *J Nucl Med* **57**, 395–395 (2016).

58. Ertay, T., Sencan Eren, M., Karaman, M., Oktay, G. & Durak, H. 18F-FDG-PET/CT in Initiation and Progression of Inflammation and Infection. *Mol Imaging Radionucl Ther* **26**, 47–52 (2017).

59. Bhambhvani, P. Challenges of cardiac inflammation imaging with F-18 FDG positron emission tomography. *J. Nucl. Cardiol.* **24**, 100–102 (2017).

60. Gigengack, F. *et al.* Motion Correction in Dual Gated Cardiac PET Using Mass-Preserving Image Registration. *IEEE Transactions on Medical Imaging* **31**, 698–712 (2012).

61. Vengrenyuk, Y. *et al.* A hypothesis for vulnerable plaque rupture due to stress-induced debonding around cellular microcalcifications in thin fibrous caps. *PNAS* **103**, 14678–14683 (2006).

62. Blau, M., Ganatra, R. & Bender, M. A. 18 F-fluoride for bone imaging. *Semin Nucl Med* **2**, 31–37 (1972).

63. Rothenberg, M. L., Nelson, A. R. & Hande, K. R. New Drugs on the Horizon: Matrix Metalloproteinase Inhibitors. *STEM CELLS* **17**, 237–240 (1999).

64. Jacobsen, J. A., Major Jourden, J. L., Miller, M. T. & Cohen, S. M. To bind zinc or not to bind zinc: An examination of innovative approaches to improved metalloproteinase inhibition. *Biochimica et Biophysica Acta (BBA) - Molecular Cell Research* **1803**, 72–94 (2010).

65. Recombinant Proteins - an overview | ScienceDirect Topics. https://www.sciencedirect.com/topics/neuroscience/recombinant-proteins.

66. Poreba, M. *et al.* Highly sensitive and adaptable fluorescence-quenched pair discloses the substrate specificity profiles in diverse protease families. *Scientific Reports* **7**, 43135 (2017).

67. Knight, C. G., Willenbrock, F. & Murphy, G. A novel coumarin-labelled peptide for sensitive continuous assays of the matrix metalloproteinases. *FEBS Letters* **296**, 263–266 (1992).

68. Fields, G. B. Using Fluorogenic Peptide Substrates to Assay Matrix Metalloproteinases. in *Matrix Metalloproteinase Protocols* (ed. Clark, I. M.) 393–433 (Humana Press, 2010). doi:10.1007/978-1-60327-299-5_24.

69. Ogata, Y., Itoh, Y. & Nagase, H. Steps Involved in Activation of the Pro-matrix Metalloproteinase 9 (Progelatinase B)-Tissue Inhibitor of Metalloproteinases-1 Complex by 4-Aminophenylmercuric Acetate and Proteinases. *J. Biol. Chem.* **270**, 18506–18511 (1995).

70. Cryer, P. E. Physiology and pathophysiology of the human sympathoadrenal neuroendocrine system. *N. Engl. J. Med.* **303**, 436–444 (1980).

71. Statovci, D., Aguilera, M., MacSharry, J. & Melgar, S. The Impact of Western Diet and Nutrients on the Microbiota and Immune Response at Mucosal Interfaces. *Front Immunol* **8**, (2017).

72. Fernandez, M. L. & West, K. L. Mechanisms by which Dietary Fatty Acids Modulate Plasma Lipids. *J Nutr* **135**, 2075–2078 (2005).

73. Lenglet, S., Mach, F. & Montecucco, F. Role of Matrix Metalloproteinase-8 in Atherosclerosis. *Mediators of Inflammation* https://www.hindawi.com/journals/mi/2013/659282/ (2013) doi:10.1155/2013/659282.

74. Kuzuya Masafumi *et al.* Effect of MMP-2 Deficiency on Atherosclerotic Lesion Formation in ApoE-Deficient Mice. *Arteriosclerosis, Thrombosis, and Vascular Biology* **26**, 1120–1125 (2006).

75. Peeters, W. *et al.* Collagenase matrix metalloproteinase-8 expressed in atherosclerotic carotid plaques is associated with systemic cardiovascular outcome. *Eur Heart J* **32**, 2314–2325 (2011).

76. Sluijter Joost P.G. *et al.* Matrix Metalloproteinase 2 Is Associated With Stable and Matrix Metalloproteinases 8 and 9 With Vulnerable Carotid Atherosclerotic Lesions. *Stroke* **37**, 235–239 (2006).

77. Sukhova, G. K. *et al.* Evidence for increased collagenolysis by interstitial collagenases-1 and -3 in vulnerable human atheromatous plaques. *Circulation* **99**, 2503–2509 (1999).

78. Rodriguez, J. A. *et al.* Metalloproteinases and atherothrombosis: MMP-10 mediates vascular remodeling promoted by inflammatory stimuli. *Front. Biosci.* **13**, 2916–2921 (2008).

79. Gupta, S., Batra, S. & Jain, M. Antibody Labeling with Radioiodine and Radiometals. *Methods Mol Biol* **1141**, 147–157 (2014).

Curriculum Vitae

Education

September 2017 – Present

University of Ottawa, Faculty of Medicine, Department of Biochemistry

Study emphases: Comprehensive Pharmacology, Cellular and Molecular Basis of Cardiovascular Function/Dysfunction

Masters thesis project: Preliminary Development and Evaluation of Matrix Metalloproteinase-13 Selective Radiotracers for Imaging Atherosclerosis

Advisor: Doctor Benjamin Rotstein, PhD

Thesis Advisory Committee members: Doctor Katey Rayner, PhD, and Doctor Darryl Davis, MD

January 2015 – March 2017

Lebanese American University, Molecular Biology department

Study emphases: Advances in Molecular and Cell biology, Cancer cell signaling, Targeted tumor therapy, Microbial pathogenesis, Bioinformatics, Genomics, Proteomics, and Advanced Human Genetics

Masters thesis project: The effect of Alpha-Ketoglutarate on learning and memory through the expression of BDNF in the hippocampus

Advisor: Doctor Sama Sleiman, PhD
Thesis Advisory Committee members: Doctor Ralph Abi Habib, PhD, and Doctor Roy Khalaf, PhD

February 2011 – May 2014

Lebanese American University, BSc in Biology

- Study emphases: Cell and Molecular biology, Microbiology, Genetics, Biochemistry, Biotechnology, Anatomy and Physiology, Virology and Immunology, Ecology
- Senior study: The effect of Anthrax lethal toxin on the MAPK in SW837 colon cancer cell lines

Supervisor: Dr Ralph Abi Habib, PhD

October 1994 - June 2009

College des Soeurs des Saints Coeurs, Hadat, Double Baccalaureate degree

Degrees: Lebanese Baccalaureate, Life Sciences division

French Baccalaureate, Specialization in Biology

Publications

April 2019

Current and future cardiovascular PET radiopharmaceuticals

Rami Al Haddad, Uzair Ismailani, Benjamin Rotstein

PET Clin. 2019 Apr;14(2):293-305

Exercise promotes the expression of brain derived neurotrophic factor (BDNF) through the action of the ketone body β-hydroxybutyrate.

Sama F Sleiman, Jeffrey Henry, Rami Al Haddad, Lauretta El Hayek, Edwina Abou Haidar, Thomas

Stringer, Devyani Ulja, Saravan S Karuppangounder, Edward Holson, Rajiv R Ratan, Ipe Ninan, Moses V Chao

Elife. 2016 Jun 2;5. pii: e15092

Mice on wheels show how exercise benefits the brain (Neuroscience news)

June 2nd, 2016

April 2016

Epigenetic changes in diabetes

Rami Al Haddad, *Nabil Karnib, Rawad Abi Assaad, Yara Bilen, Nancy Emmanuel, Anthony Ghanem, Joe Younes, Victor Zibara, Sama F Sleiman*
Neurosci Lett. 2016 Jun 20;625:64-9

Research experience

May 2017 – Present

Graduate student/MSc Thesis

Dr Benjamin Rotstein's lab, University of Ottawa Heart Institute

The research in Dr Rotstein's lab focuses on the molecular imaging of dynamic biochemical processes is used to study normal and diseased conditions, evaluate response to therapy, and for clinical diagnosis. Radiotracers for positron emission tomography (PET) contain short-lived radioactive isotopes and engage in highly specific and selective molecular interactions with enzyme or receptor targets in vivo. Radiotracer development therefore demands a confluence of understanding of biochemical processes and targets, medicinal chemistry and probe design, synthetic and radiochemistry, as well as pharmacology and imaging analysis. From a foundation in all aspects of radiopharmaceutical chemistry, most projects in the lab seek to develop strategies and methods for application ultimately in nuclear molecular imaging research and clinical diagnosis.

My job in Doctor Rotstein's lab is to assess enzyme specificities and dynamics, handle animal work and PET imaging for all other projects, perform en face aorta autoradiography studies. In addition, I was involved in other cellular and clinical projects in the lab and in collaboration with other labs. During this time, I was able to publish one review paper and is in the process of completing my project for publication.

Technical skills:

Radiochemistry: Radiolabelling of MMP-13 inhibitor for use in PET and autoradiography

Nuclear imaging: PET scans on mice and rats, autoradiography on en face aorta, biodistribution of radiolabelled tracer in essential organs using gamma counter

Dissections: Harvesting of adult mice aortas and other essential organs

Cellular biology: Cell culture: MCF-7 and MDA-MB-231

Jul 2015 – March 2017

Research Assistant

Dr Sama Sleiman's lab, Lebanese American University

The research work in Dr Sleiman's lab focuses on identifying both the transcriptional and posttranscriptional networks regulating neuronal death during central nervous diseases in an attempt to identify novel therapeutic targets. Dr Sleiman's research group is also interested in understanding how physical exercise induces beneficial responses in the brain and ameliorates the symptoms of depression. Three major projects are understudy: 1) Deciphering the epigenetic pathways, particularly the role of histone deacetylases in neuronal death during both chronic and acute insults to the central nervous system. 2) Identifying the post-transcriptional networks induced

by neurotoxic stress, specifically the microRNAs involved in the regulation of neuronal death during disease. 3) Understanding how physical exercise induces BDNF expression in the hippocampus to mediate its positive effects on memory formation and synaptic plasticity.

In Dr Sleiman's lab, I was the first student she had and was the one who developed and optimized all of the experiments that were done and still being done nowadays. I have been working intensively on isolating mouse embryos hippocampal sections of primary cell studies and different behavioral experiments.

Technical Skills

Cellular biology: Cell culture: Neuronal cultures preparation from E18 mice embryos

Biochemistry: Western blot, Chromatin IP

Analytical methods: RNA extraction, DNA extraction, Reverse transcription PCR, Real time PCR, Protein extraction and quantification methods

Behavioral experiments: Water maze assay, Social defeat assay

Dissections: Dissection of adult mice brains and differentiation of each part, dissection of E18 mice brains.

Sep 2013 - May 2014

Senior study student

Dr Ralph Abi Habib's lab, Lebanese American University

The research interests in Dr Abi Habib's lab include the molecular mechanisms of carcinogenesis, identification of selectable tumor markers, selective targeting of tumor cells and the development of tumor-selective fusion toxins for the treatment of solid and hematological malignancies. His research work has been published in conference presentations and international journals, and it has been acknowledged internationally.

My senior study class was with Dr Abi Habib's lab. I was able to learn some techniques (culturing cancer cells, flow cytometry…), write a review paper, and present another paper.

Teaching experience:

September 2018 – April 2019

Teaching assistant

Department of Chemistry and Biomolecular Sciences (French sections), University of Ottawa

General chemistry lab instructor (*September 2018 – December 2018*), Organic chemistry lab instructor (*January 2019 – April 2019*), and Biochemistry lab instructor (*January 2019 - April 2019*)

Teaching lab sessions, answering students' questions and performing lab experiments, preparing lessons and experiment material, setting up, correcting, and grading lab reports.

Jan 2015 – May 2017

Lab instructor/Graduate assistant

Department of Natural Sciences, Lebanese American University

Genetics lab coordinator and instructor (September 2015 - December 2016), and instructor and graduate assistant in Biology introductory labs (January 2017 - May 2017),

Teaching lab sessions, answering students' questions and performing lab experiments, preparing lessons and experiment material, setting up, correcting, and grading exams and lab reports.

The graduate assistant position also includes proctoring several exams per semester.

Feb 2011 - May 2014

Senior assistant

Chemistry lab, Lebanese American University

My tasks in the chemistry lab were mainly assisting lab instructors, preparing solutions, calibrating lab instruments, and organizing lab equipment for lab sessions.

Honours and Awards

July 2019

University of Ottawa Financial Aid Bursary (international students)

June 2019

CUPE Employees Financial Aid/Local 2626 (for international students) - Spring/Summer

November 2018

University of Ottawa Financial Aid Bursary (international students)

November 2018

CUPE Employees Financial Aid/Local 2626 (for international students) – Fall

May 2018

University of Ottawa Financial Aid Bursary (international students)

March 2018

CUPE Employees Financial Aid/Local 2626 (for international students) – Winter

November 2017

University of Ottawa Financial Aid Bursary (international students)

Academic and administrative experience:

May 2019 – Present

Heart institute representative, Biochemistry, Microbiology, Immunology Graduate Student Association (BMIGSA)

Representing the University of Ottawa Heart Institute in the graduate student council of the BMI department and the school of medicine, ensuring the presence and maintenance of a constant connection between the different departments of the School of Medicine.

Conferences

Canadian Chemistry Conference and Exhibition (CCCE), Quebec City, *June 2019*:

Preliminary Development and Evaluation of Matrix Metalloproteinase-13 Selective Radiotracers for Imaging Atherosclerosis (Poster), Quebec City Convention Centre

Toronto - Ottawa Cardiovascular Research Day, Ottawa, *May 2019:*

Preliminary Development and Evaluation of Matrix Metalloproteinase-13 Selective Radiotracers for Imaging Atherosclerosis (Poster), National Arts Centre

7th International Ottawa Heart Conference, Ottawa, *April 2019:*

Preliminary Development and Evaluation of Matrix Metalloproteinase-13 Selective Radiotracers for Imaging Atherosclerosis (Poster), University of Ottawa Heart Institute

University of Ottawa Biochemistry, Microbiology, Immunology Seminar day, Ottawa, *February 2019:*

Preliminary Evaluation of Matrix Metalloprotienase-13 as a Target for Imaging Atherosclerosis (Oral presentation), University of Ottawa, Faculty of Medicine

University of Ottawa Biochemistry, Microbiology, Immunology Poster day, Ottawa, *May 2018:*

Preliminary Development and Evaluation of Selective MMP-13 radiotracers for Imaging Atherosclerosis (Poster), University of Ottawa, Faculty of Medicine

University of Ottawa Biochemistry, Microbiology, Immunology Scientific Symposium, Ottawa, *May 2018:*

Preliminary Development and Evaluation of Selective MMP-13 radiotracers for Imaging Atherosclerosis (Poster), University of Ottawa, Faculty of Medicine

Lebanese American University Scientific Poster Day, Byblos, Lebanon, *March 2016:*

Role of β-hydroxybutyrate in Neuronal Plasticity and Cognition (Poster), Lebanese American University, Faculty of Natural Sciences

Lebanese American University Scientific Poster Day, Byblos, Lebanon, *March 2016:*

Lactic Acid Effect on the Expression of BDNF (Poster), Lebanese American University, Faculty of Natural Sciences

Lebanese American University Scientific Poster Day, Byblos, Lebanon, *March 2016:*

Brain Derived Neurotrophic Factor Induction by α-Ketoglutarate (Poster), Lebanese American University, Faculty of Natural Sciences

Skills and Qualifications

Languages:

Arabic: Lebanese Dialect as mother language

French: Fluent, French Baccalaureate in French accredited high school

English: Business-fluent, Higher education in an American institution, Lebanese American University

Strong communication and presentation skills: presenting data clearly and confidently to small and large groups, ability to modify content to suit the understanding of others.

Computer skills: Very good knowledge of PubMed, BD Accun C6 Flow Cytometer Software, Gen5RC reader control software, Gen5, GraphPad Prism 5 and NCBI Standard Protein BLAST; Good knowledge of Ensembl Genome Browser, Uniprot

Arts:

Piano:

12 years of Piano studies in the Lebanese National Conservatory for Higher Music Education

Community services:

Red Cross paramedic (*May 2013 – March 2017*)

Youth as Agents of Behavioral Change facilitator (*December 2013 – March 2017*)